Mon. Not. R. Astron. Soc. **000**, 000–000 (0000) Printed February 20, 2015 (MN LATEX style file v2.2)

# Evolution of the atomic and molecular gas content of galaxies in dark matter haloes

Gergö Popping[1,2⋆], Peter S. Behroozi[3] and Molly S. Peeples[3]
[1] *Kapteyn Astronomical Institute, University of Groningen, Postbus 800, NL-9700 AV Groningen, the Netherlands,*
[2] *European Southern Observatory, Karl-Schwarzschild-Strasse 2, 85748, Garching, Germany*
[3] *Space Telescope Science Institute, Baltimore, MD 21218 USA*

arXiv:1409.1574v2 [astro-ph.GA] 19 Feb 2015

February 20, 2015

**ABSTRACT**

We present a semi-empirical model to infer the atomic and molecular hydrogen content of galaxies as a function of halo mass and time. Our model combines the SFR–halo mass–redshift relation (constrained by galaxy abundances) with inverted SFR–surface density relations to infer galaxy H I and $H_2$ masses. We present gas scaling relations, gas fractions, and mass functions from $z = 0$ to $z = 3$ and the gas properties of galaxies as a function of their host halo masses. Predictions of our work include: 1) there is a $\sim 0.2$ dex decrease in the H I mass of galaxies as a function of their stellar mass since $z = 1.5$, whereas the $H_2$ mass of galaxies decreases by $> 1$ dex over the same period. 2) galaxy cold gas fractions and $H_2$ fractions decrease with increasing stellar mass and time. Galaxies with $M_\star > 10^{10}\,M_\odot$ are dominated by their stellar content at $z \leqslant 1$, whereas less-massive galaxies only reach these gas fractions at $z = 0$. We find the strongest evolution in relative gas content at $z < 1.5$. 3) the SFR to gas mass ratio decreases by an order of magnitude from $z = 3$ to $z = 0$. This is accompanied by lower $H_2$ fractions; these lower fractions in combination with smaller gas reservoirs correspond to decreased present-day galaxy SFRs. 4) an $H_2$-based star-formation relation can simultaneously fuel the evolution of the cosmic star-formation and reproduce the observed weak evolution in the cosmic H I density. 5) galaxies residing in haloes with masses near $10^{12}\,M_\odot$ are most efficient at obtaining large gas reservoirs *and* forming $H_2$ at all redshifts. These two effects lie at the origin of the high star-formation efficiencies in haloes with the same mass.

**Key words:** galaxies: evolution - galaxies: formation - galaxies: ISM - ISM: molecules - ISM: atoms

## 1 INTRODUCTION

Understanding of the gas evolution of galaxies provides fundamental constraints on our theories for galaxy formation and evolution. The star formation (SF) in a galaxy is regulated by the amount of cold gas eligible to form stars. Observations have shown a strong correlation between star-formation rate (SFR) surface density and the density of molecular hydrogen out to $z \sim 2$ (Wong & Blitz 2002; Bigiel et al. 2008; Daddi et al. 2010; Genzel et al. 2010; Bigiel & Blitz 2012). Locally, the correlation of SFR surface density with atomic hydrogen is weak (Bigiel et al. 2008; Leroy et al. 2008). These results suggest that before forming stars, cool gas that accretes onto a galaxy must go through an atomic and molecular phase. Knowledge of the cold gas content of galaxies and its partitioning into H I and $H_2$ therefore provides valuable constraints on the physics that control this baryonic cycle.

Abundance matching techniques and empirical models have shown that haloes with masses near $10^{12}\,M_\odot$ are most efficient at forming stars and that the star-formation histories for galaxies with varying $z = 0$ halo mass are very different (e.g., Yang, Mo & van den Bosch 2003; Conroy & Wechsler 2009; Behroozi, Conroy & Wechsler 2010; Guo et al. 2010; Moster et al. 2010; Wang & Jing 2010; Yang et al. 2012; Behroozi, Wechsler & Conroy 2013b; Moster, Naab & White 2013; Reddick et al. 2013; Lu et al. 2014b,c). The halo mass dictates the gas supply onto a galaxy. It is therefore crucial to couple the cold gas content of a galaxy to the halo framework, in order to fully understand the physics that translates the supply of cold gas into the stellar buildup of galaxies and constrain processes such as winds, heating, and cooling.

Large surveys of the cold gas content in galaxies have

⋆ E-mail: gpopping@eso.org

mainly been restricted to our local Universe. Atomic hydrogen surveys such as ALFALFA (Giovanelli et al. 2005), THINGS (The HI Nearby Galaxy Survey; Walter et al. 2008), GASS (GALEX Arecibo SDSS survey; Catinella et al. 2010, 2012, 2013) and molecular hydrogen surveys (typically through CO emission) such as BIMA SONG (Bima survey of nearby galaxies; Helfer et al. 2003), HERACLES (HERA CO-Line Extragalactic Survey; Leroy et al. 2009), and COLD GASS (CO legacy database for GASS; Saintonge et al. 2011) have mapped the H I and $H_2$ content of local galaxies, providing constraints on the gas-to-star ratios and H I and $H_2$ mass function of galaxies. These surveys have provided important insights into the connections between stellar mass, star formation rate and gas properties of galaxies, but do not probe the evolution in galaxy gas properties that drive the stellar buildup of galaxies.

Observations of atomic gas in emission in galaxies have been restricted to $z \leqslant 0.25$ (Verheijen et al. 2007; Catinella et al. 2008; Catinella & Cortese 2015). As a pilot for CHILES (Cosmos H I Legacy Survey), Fernández et al. (2013) observed H I in emission in 33 galaxies in the redshift interval $0 < z < 0.19$. Damped Lyman-$\alpha$ absorbers (DLAs) have provided an alternative approach to estimate the global gas content in galaxies up to much higher redshifts ($z < 4$; e.g., Rao, Turnshek & Nestor 2006; Prochaska & Wolfe 2009; Noterdaeme et al. 2012; Zafar et al. 2013), but the nature of DLAs and their connection to galaxies is still unclear (Berry et al. 2014).

Over the past years a wealth of direct observations of $H_2$ (through CO) in high-redshift galaxies have become available, although usually biased towards gas-rich, actively star-forming galaxies (e.g., Daddi et al. 2010; Tacconi et al. 2010; Genzel et al. 2010; Geach et al. 2011; Riechers et al. 2011; Bauermeister et al. 2013; Tacconi et al. 2013). Although results from these surveys are still inconclusive because of small and biased samples, these studies suggest that galaxies at high-redshift may have had larger molecular hydrogen reservoirs than local counterparts. The above efforts have led to valuable insights and constraints on galaxy formation models, but still show a very limited picture of the evolution of cold gas in galaxies. We anticipate that the newest generation of radio and sub-mm instruments such as ALMA, SKA and its pathfinders MeerKat and ASKAP will improve the number statistics and revolutionize our understanding of the gas properties of galaxies over cosmic time.

Indirect estimates of the total gas and/or $H_2$ mass of large samples of galaxies at high redshift (Erb et al. 2006; Mannucci et al. 2009; Popping et al. 2012, Popping et al. in prep.) have improved the number statistics but still suffer from severe selection criteria. These studies were not in the position to address the H I and $H_2$ mass function, nor the cosmic density of cold gas. Furthermore, they lack the capability to probe the connection between a galaxy's halo and cold gas content.

In the last decade significant progress has been made on developing models that track the H I and $H_2$ content of galaxies (e.g., Obreschkow et al. 2009; Dutton, van den Bosch & Dekel 2010; Fu et al. 2010; Lagos et al. 2011; Christensen et al. 2012; Krumholz & Dekel 2012; Kuhlen et al. 2012; Davé et al. 2013; Popping, Somerville & Trager 2014; Rafieferantsoa et al. 2014; Thompson et al. 2014). These models have proven to be very successful in reproducing the available observational constraints on the H I, $H_2$ and sub-mm (Popping et al. 2014) properties of galaxies in the local and high-redshift Universe. Despite this success, theoretical models still have a hard time reproducing stellar-to-halo mass ratios at $z > 0$ (Lu et al. 2014a) and the star-formation history of low-mass galaxies (Weinmann et al. 2012; Somerville & Davé 2014). Additional information on the gas content of galaxies in haloes will be crucial to break degeneracies in different physical mechanisms included in models such as supernovae feedback, metal enrichment, feedback from active galactic nuclei and shock heating.

In this paper we present a new semi-empirical approach to constrain the H I and $H_2$ content of galaxies as a function of time and halo mass in the redshift range $z = 0 - 3$. We couple a sub-halo abundance matching model (SHAM) (Behroozi, Wechsler & Conroy 2013a,b) with a model to indirectly estimate the H I and $H_2$ content of a galaxy (Popping et al. 2012). With our approach we can follow galaxy gas properties as a function of time and halo mass. It provides an unique opportunity to infer galaxy H I and $H_2$ masses, mass functions, and cosmic densities out to $z = 3$. This allows us to gain insights into the processes that shape the maximum star-formation efficiency in haloes with $M_{\rm vir} \sim 10^{12}\,{\rm M}_\odot$ and study the gas properties of galaxies that drive the peak in cosmic SFR density at $z \sim 2$ (e.g. Hopkins & Beacom 2006; Madau & Dickinson 2014). We aim to provide constraints for the gas content of galaxies to be observed with the newest generation of radio and sub-mm instruments and at the same time provide valuable constraints for galaxy formation models. One of the main benefits in choosing this approach is that galaxy gas masses are based on star-formation histories that *by construction* are representative of real galaxies. The presented approach is in stark contrast to semi-analytical models. Instead of having to introduce uncertain recipes for the formation and evolution of galaxies, we can focus on the galaxy gas content within a realistic framework. Similar techniques have been used to look at the evolution of the stellar metallicity and galaxy age (Peeples & Somerville 2013; Muñoz & Peeples 2014) and the in- and outflow of gas in galaxies (Lu, Mo & Lu 2014). Because our approach is based on realistic star-formation histories, the inferred gas properties provide very useful predictions for future observations.

This paper is organized as follows. In Section 2 we present our methodology. In Section 3 we present our results and we discuss them in Section 4. We summarize our findings in Section 5. Throughout this paper we assume a flat $\Lambda$ cold dark matter ($\Lambda$CDM) cosmology with $H_0 = 70\,{\rm km\,s^{-1}}$, $\Omega_{\rm matter} = 0.27$, $\Omega_\Lambda = 0.73$, $n_s = 0.95$, and $\sigma_8 = 0.82$ (Behroozi, Wechsler & Conroy 2013b). We assume a Chabrier stellar initial mass function (IMF: Chabrier 2003) in the mass range $0.1 - 100\,{\rm M}_\odot$ and where necessary convert observational quantities used to a Chabrier IMF. All presented gas masses are pure hydrogen masses. Unless noted different, presented gas masses do not include a correction for Helium.

## 2 METHODOLOGY

This section describes our methodology to model the gas content of galaxies. We will first give a short overview of

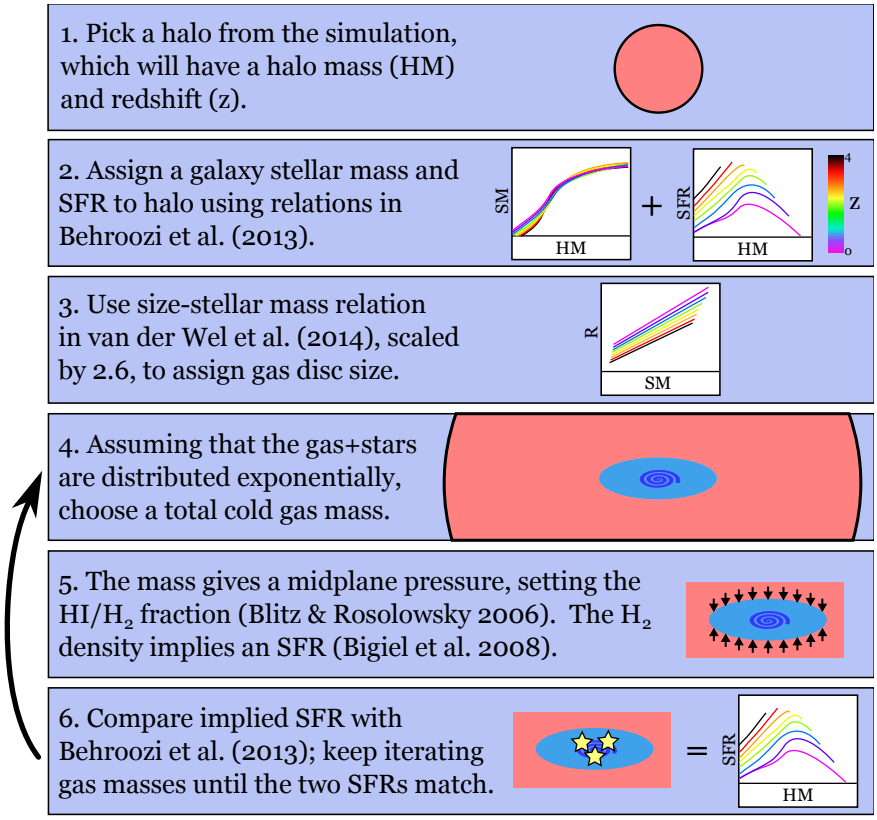
1. Pick a halo from the simulation, which will have a halo mass (HM) and redshift (z).
2. Assign a galaxy stellar mass and SFR to halo using relations in Behroozi et al. (2013).
SM
HM
+
SFR
HM
Z
3. Use size-stellar mass relation in van der Wel et al. (2014), scaled by 2.6, to assign gas disc size.
R
SM
4. Assuming that the gas+stars are distributed exponentially, choose a total cold gas mass.
5. The mass gives a midplane pressure, setting the HI/H2 fraction (Blitz & Rosolowsky 2006). The H2 density implies an SFR (Bigiel et al. 2008).
6. Compare implied SFR with Behroozi et al. (2013); keep iterating gas masses until the two SFRs match.
=
SFR
HM

**Figure 1.** A flowchart of the methodology used to estimate the H I and $H_2$ masses of galaxies based on realistic star-formation histories.

the SHAM used to provide SFRs, stellar masses, and halo masses in Section 2.1. We will then describe our method to estimate the gas masses of galaxies in Section 2.2. We present a schematic overview of this model and its main individual ingredients in Figure 1. The individual steps depicted in Figure 1 are described below.

### 2.1 Sub-halo abundance matching

We use the abundance modeling approach in (Behroozi, Wechsler & Conroy 2013b) to provide star-formation histories (halo mass, stellar mass, and SFR as a function of redshift) that by construction are representative of real galaxies. The abundance modeling approach adopts a very flexible parametrization for the stellar mass–halo mass relationship as a function of redshift, $M_\star(M_{\rm vir}, z)$. This parametrization has six variables to control the normalization and shape of the relationship (a characteristic stellar mass, halo mass, faint-end slope, massive-end cutoff, transition region shape, and scatter); for each variable, three parameters control the redshift scaling at low ($z = 0$), mid ($z \sim 1$) and high ($z > 3$) redshift. This results in a total of eighteen shape parameters. Additional nuisance parameters account for systematic observational biases in how galaxy luminosities are converted to stellar masses/star formation rates. A specific choice of $M_\star(M_{\rm vir}, z)$ applied to a dark matter simulation results in an assignment of a galaxy stellar mass to every halo at every redshift in the simulation. By counting galaxies at individual redshifts, and by tracing the growth of galaxies along dark matter halo merger trees, this assignment yields concrete predictions for observed stellar mass functions, cosmic star formation rates, and specific star formation rates. Comparing these predictions to observed data (i.e., stellar mass functions and star formation rates) from $z = 0$ to $z \sim 8$ results in a likelihood for a given choice of $M_\star(M_{\rm vir}, z)$. The posterior distribution for $M_\star(M_{\rm vir}, z)$, along with derived values for the average star formation rate as a function of halo mass and redshift, are then inferred from observed data using an MCMC approach. The full details of this method are presented in Behroozi, Wechsler & Conroy (2013b).

The average SFRs include a contribution from actively star-forming and quenched galaxies. In this paper we are particularly interested in star-forming galaxies. To estimate the fraction of quenched galaxies we use the fitting formula by Brammer et al. (2011)

$$f_{\rm quenched}(M_\star, z) = \left[\left(\frac{M_\star}{10^{10.2+0.5z}\,M_\odot}\right)^{-1.3} + 1\right]^{-1}. \quad (1)$$

Beyond $z = 3$ all galaxies are considered to actively form stars (i.e., $f_{\rm quenched} = 0$). Under the assumption that the contribution from quenched galaxies to the average SFR is negligible we can estimate the SFR of actively star-forming galaxies as $SFR_{\rm active} = SFR_{\rm average} / (1 - f_{\rm quenched})$. Combined with the evolution of the SFR – stellar mass relation, this quenched fraction evolution accurately reproduces the distribution of ages of local galaxies (Muñoz & Peeples 2014).

To reproduce the observed scatter in the relation between stellar mass and SFR we calculate the gas masses for each halo mass–stellar mass–SFR realization multiple times

with a scatter in SFR of 0.3 dex (e.g., Noeske et al. 2007). We assume a scatter in the stellar masses at fixed halo mass of $\xi = 0.218 - 0.023(a-1)$ dex, where $a$ is the cosmological scale factor. On top of that we assume that the observational uncertainty around the stellar masses is log-normal, with a redshift dependent standard deviation $\sigma(z) = \sigma_0 + \sigma_z z$, where $\sigma_0 = 0.07$ and $\sigma_z = 0.061$ (Behroozi, Wechsler & Conroy 2013b).

Halo mass functions used in this work are taken from the fitting functions in Behroozi, Wechsler & Conroy (2013b), which are based on the fits in Tinker et al. (2008). Halo masses are defined as spherical overdensities according to the virial overdensity criterion of Bryan & Norman (1998).

### 2.2 Indirect gas measures

We infer the H I and $H_2$ content of a galaxy based on the approach presented in Popping et al. (2012). This method uses the combination of an empirical molecular-based SF relation (based on Bigiel et al. 2008) and a pressure-based prescription to calculate the $H_2$-to-H I surface-density ratio of cold gas (Blitz & Rosolowsky 2006). We pick a gas mass and solve for the SFR using the set of equations described below. We then iterate through gas masses till convergence with the SFR picked from Behroozi, Wechsler & Conroy (2013b) is reached.

We use a slightly adapted version of the molecular-based SFR relation deduced in Bigiel et al. (2008) to allow for higher star-formation efficiencies in high gas surface density regions. This is motivated by the results of Daddi et al. (2010) and Genzel et al. (2010), who found that the SFR surface density relation at high densities has a slope of 1.4 (versus 1 in Bigiel et al. 2008). The adopted equation is given by

$$\Sigma_{\rm SFR} = \frac{A_{\rm SF}}{10 {\rm M}_\odot\,{\rm pc}^{-2}} \left(1 + \frac{\Sigma_{\rm gas}}{\Sigma_{\rm crit}}\right)^{N_{\rm SF}} f_{\rm H_2}\,\Sigma_{\rm gas} \quad (2)$$

where $\Sigma_{\rm SFR}$ and $\Sigma_{\rm gas}$ are the star formation and cold gas surface densities in ${\rm M}_\odot\,{\rm yr}^{-1}\,{\rm kpc}^{-2}$ and ${\rm M}_\odot\,{\rm pc}^{-2}$, respectively; $A_{\rm SF}$ is the normalization of the power law in ${\rm M}_\odot\,{\rm yr}^{-1}\,{\rm kpc}^{-2}$; $\Sigma_{\rm crit}$ is the critical surface density above which the star formation follows Kennicutt (1998); $N_{\rm SF}$ is an index which sets the efficiency; and $f_{\rm H_2} = \Sigma_{\rm H_2}/(\Sigma_{\rm HI}+\Sigma_{\rm H_2})$ is the local molecular gas fraction. Following Popping et al. (2012) we use $N_{\rm SF} = 0.5$ and $\Sigma_{\rm crit} = 100\,{\rm M}_\odot\,{\rm pc}^{-1}$. When not accounting for the increased star-formation efficiency of high surface density regions (i.e. $N_{\rm SF} = 0$) we infer 10 percent more gas in galaxies with ${\rm SFR}/(2\pi {\rm r}_\star^2) \approx 1\,{\rm M}_\odot\,{\rm yr}^{-1}\,{\rm kpc}^{-2}$ and roughly 75 percent more gas in galaxies with ${\rm SFR}/(2\pi {\rm r}_\star^2) \approx 10\,{\rm M}_\odot\,{\rm yr}^{-1}\,{\rm kpc}^{-2}$.

We calculate the molecular fraction of the cold gas using a pressure-regulated recipe to determine the molecular fraction of the cold gas, based on the work by Blitz & Rosolowsky (2006). The authors found a power-law relation between the mid-plane pressure acting on a galaxy disc and the ratio between molecular and atomic hydrogen, i.e.,

$$R_{\rm H_2} = \left(\frac{\Sigma_{\rm H_2}}{\Sigma_{\rm HI}}\right) = \left(\frac{P_m}{P_0}\right)^\alpha \quad (3)$$

where $P_0$ is the external pressure in the interstellar medium where the molecular fraction is unity and $\alpha$ is the power-law index. We use $P_0 = 3.25 \times 10^{-13}{\rm erg\,cm}^{-3}$ and $\alpha = 0.8$, based on the results presented in Leroy et al. (2008). $P_m$ is the mid-plane pressure acting on the galaxy disc. Following Popping et al. (2012) we describe the mid-plane pressure by

$$P_m(r) = \frac{\pi}{2}\,G\,\Sigma_{\rm gas}(r)\left[\Sigma_{\rm gas}(r) + 0.1\sqrt{\Sigma_\star(r)\Sigma_{\star,0}}\right], \quad (4)$$

where G is the gravitational constant, $r$ is the radius from the galaxy centre, and $\Sigma_{\star,0} \equiv M_\star/(2\pi r_\star^2)$, based on empirical scalings for nearby disc galaxies. We now have all the necessary ingredients to calculate $R_{\rm H_2}$ and subsequently the cold gas molecular fraction [$f_{\rm H_2} = R_{\rm H_2}/(1+R_{\rm H_2})$].

We assume that cold gas and stars are distributed following an exponential profile[1]. We estimate the disc scale length $r_\star$ as a function of stellar mass and redshift by linearly interpolating through the fits presented in Table 2 in van der Wel et al. (2014). Stellar disc sizes increase with stellar mass and time. For galaxies with stellar masses less than $10^9\,{\rm M}_\odot$ we estimate the disc scale length based on work by Kravtsov (2013), who relates the scale length of a disc to the size of its host halo. The typical uncertainty given by van der Wel et al. (2014) is 0.2 dex. Following Kravtsov (2013) we assume that the scale length of the gaseous disc is 2.6 times larger than the scale length of the stellar disc. Varying $\chi_{\rm gas}$ results in negligible differences in inferred cold gas and $H_2$ mass as long as $\chi_{\rm gas} > 1$. Decreasing $\chi_{\rm gas}$ to values less than one leads to more significant differences in the inferred gas masses. When adopting $\chi_{\rm gas} = 0.5$ we find that the inferred gas and molecular masses are lowered by 0.25 and 0.1 dex, respectively. Observations of the sizes of the CO discs of galaxies at $z \sim 1.2$ and $z \sim 2.2$ (supposedly tracing the molecular hydrogen) do not support a scale length ratio of $\chi_{\rm gas} \ll 1.0$ (e.g., Tacconi et al. 2010, 2013). Resolved observations of CO discs with ALMA will be able to better address the scale length ratio between the stellar and molecular disc of galaxies at high redshifts.

The assumption of an exponential disc morphology may not be physical for galaxies at $z = 0$ with stellar masses below $\sim 10^9\,{\rm M}_\odot$ (Kelvin et al. 2014). At higher redshifts it is unclear at which stellar mass the assumption of disc structure may break down. As a consequence, assuming that the distribution of gas in irregular galaxies is clumpy, the inferred H I content of galaxies in this mass regime may be too high. The inferred H I disc mass for satellites may also be overestimated if these galaxies undergo significant stripping.

We calibrated our method using direct observations of the H I and/or $H_2$ content of galaxies in the local and high-redshift Universe from Leroy et al. (2008), Daddi et al. (2010), Tacconi et al. (2010), and Tacconi et al. (2013). Using $\chi^2$-minimization, we find best agreement between inferred and observed gas masses for this sample when adopting a value of $A_{\rm SF} = 9.6 \times 10^{-3}\,{\rm M}_\odot\,{\rm yr}^{-1}\,{\rm kpc}^{-2}$ for the efficiency of forming stars out of molecular gas. We integrate the disc out to a hydrogen column density of $N_H = 10^{18}\,{\rm cm}^{-2}$ (the cold gas at these column densities is atomic). The adopted value for $A_{\rm SF}$ is within the errors on $A_{\rm SF}$ in Bigiel et al. (2008) and Bigiel & Blitz (2012). The cut in hydrogen

[1] This is slightly different from Popping et al. (2012), where the star formation was assumed to follow an exponential distribution rather than the cold gas.

column density at $N_H = 10^{18}\,\mathrm{cm}^{-2}$ affects the inferred H I masses by a few percent in galaxies with global SFR surface density (defined as $\mathrm{SFR}/[2\pi r_\star^2]$) less than $10^{-4}$ with respect to the approach adopted in Popping et al. (2012).

Popping et al. (2012) showed that this method is very successful in reproducing the cold gas and $H_2$ surface densities of local galaxies and the integrated H I and/or $H_2$ mass of local and high-redshift galaxies. We refer the reader to the Popping et al. paper for a more detailed description of this method, including uncertainties in the free parameters. The typical systematic uncertainty for the inferred gas masses (based on uncertainties in $\chi_{\mathrm{gas}}$, the star-formation efficiency, and the parameters that control the partitioning of cold gas in an atomic and molecular component) is 0.25 dex.

### 2.3 Distribution of inferred gas masses for fixed halo mass

This work is based on several relations with different underlying distributions and uncertainties. To develop a feeling of the effect that these underlying distributions have on the inferred gas masses, we show the histograms of the distributions of inferred H I and $H_2$ masses for fixed halo masses at $z = 0.0$ in Figure 2. We find that the distribution in H I and $H_2$ masses is typically log-normal. The distribution in H I has a width of $\sim 0.45$ dex, independent of host halo mass. The $H_2$ distribution has a width of $\sim 0.45$ and $\sim 0.6$ dex for galaxies residing in haloes with masses of $10^{11-12}\,\mathrm{M}_\odot$ and $10^{13-14}\,\mathrm{M}_\odot$, respectively.

## 3 RESULTS

In this Section we present our inferred gas masses for galaxies in the local and high-redshift Universe. We compare our results to observations of local and high-redshift galaxies in Section 3.1. We present predictions for future H I and $H_2$ surveys of galaxies at $z > 0$ in Section 3.2. We finish by discussing the gas properties of galaxies as a function of their halo mass in Section 3.3. In all figures the solid line and the shaded regions mark the mean and one standard deviation of the posterior distributions. The posterior distributions are obtained by inferring the gas masses based on a thousand different realizations for the stellar mass – halo mass relation. For each realization we infer the gas masses multiple times, to fully cover the uncertainties and distributions in SFR, stellar, mass, size, and our methodology to infer gas masses.

### 3.1 Gas in local galaxies

We present scaling relations for the total cold gas, H I and $H_2$ content of local star-forming galaxies compared to observations in Figure 3. Our observational sample ranges from local dwarf galaxies to the most actively star-forming galaxies in the local Universe including objects taken from the THINGS survey (Leroy et al. 2008; Walter et al. 2008), GASS+COLDGASS (Catinella et al. 2010; Saintonge et al. 2011), LITTLE THINGS survey (Hunter et al. 2012; Zhang et al. 2012), McGaugh (2012), Boselli et al. (2014), and the ALLSMOG survey (Bothwell et al. 2014).

We find good agreement between model and observations for the relative and absolute H I content of galaxies over the entire mass range probed. The H I mass of galaxies increases with stellar mass, but the ratio between H I and stellar mass decreases. We find an increasing trend in $H_2$ mass with stellar mass, in good agreement with observations. The relation between stellar mass and $H_2$ mass is steeper than the relation between stellar mass and cold gas and H I mass. The inferred $H_2$-to-stellar mass ratio is flat up to stellar masses of $M_\star \sim 10^{10.5}\,\mathrm{M}_\odot$ and drops afterwards. Observations suggest a continuous decline in the $H_2$-to-stellar mass ratio with stellar mass, however, the $H_2$ mass of galaxies with low stellar masses is not well constrained ($M_\star < 10^8\,\mathrm{M}_\odot$). This is partially due to small sample sizes and partially due to uncertainties in the $H_2$ mass as estimated through CO for low-metallicity objects (Schruba et al. 2011).

We compare our inferred local H I and $H_2$ mass functions to observations in Figure 4. We reach decent agreement with the observed H I mass function for galaxies with H I masses $M_{\mathrm{HI}} > 10^9\,\mathrm{M}_\odot$. Below this mass, our model finds a much steeper slope in the H I mass function than suggested by observations. The galaxies responsible for this excess have low stellar masses ($M_\star < 10^{8.5}\,\mathrm{M}_\odot$). We will further discuss this in Section 4.5.

We obtain good agreement between the observed and inferred $H_2$ mass function over the entire mass range probed. Only at the knee of the $H_2$ mass function ($M_{\mathrm{H2}} \sim 10^{9.5}$) do we slightly underpredict the number density of galaxies compared to observations.

Overall we successfully infer the gas properties of galaxies with stellar masses larger than $10^{8.5}\,\mathrm{M}_\odot$. The SHAM adopted in this work was designed to match the locally observed stellar mass function and specific star-formation rates of galaxies (Behroozi, Wechsler & Conroy 2013b). Our methodology to estimate the H I and $H_2$ masses of local galaxies was calibrated using a sample partially consisting of local gas rich objects. Although the combination of these two models does not necessarily guarantee the degree of agreement found between our model and observations, the good match is an encouraging sanity check.

### 3.2 Evolution of gas in galaxies

#### *3.2.1 Scaling relations*

We present inferred galaxy $H_2$ masses at redshifts $z \sim 0.3$, $z \sim 1.2$, and $z \sim 2.2$ in Figure 5. At these redshifts there are ample observations from the literature available to compare our model to (Tacconi et al. 2010; Bauermeister et al. 2013; Tacconi et al. 2013). We find an increasing trend in galaxy $H_2$ mass with stellar mass at all redshifts, in good agreement with observations. The relation between $H_2$ mass and stellar mass flattens for the most stellar-massive galaxies ($M_\star > 10^{11}\,\mathrm{M}_\odot$), suggestive of an upper plateau in $H_2$ mass. As for the local gas measures, our methodology was designed to properly reproduce observed stellar mass functions and SFRs in this redshift range and our indirect gas measure recipe was calibrated using among others the Tacconi et al. observations. Nevertheless, it is encouraging that our model simultaneously reproduces the available gas measures in the local and high-redshift Universe.

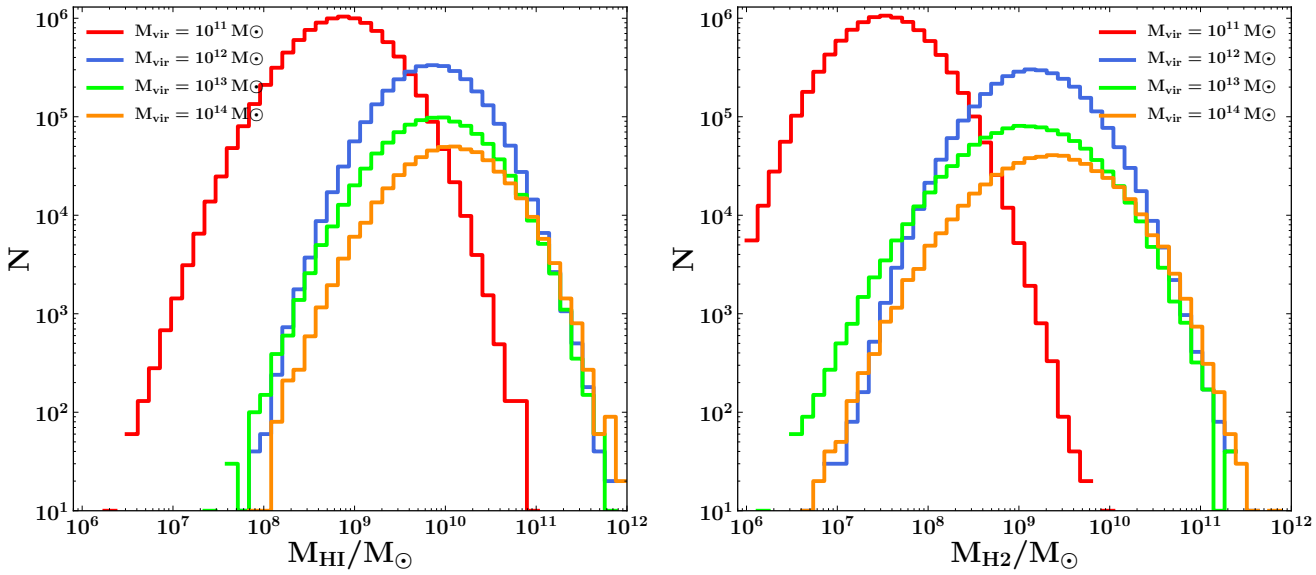


**Figure 2.** Histograms of the distribution in the inferred H I (left) and $H_2$ (right) masses for fixed halo masses at $z = 0.0$.

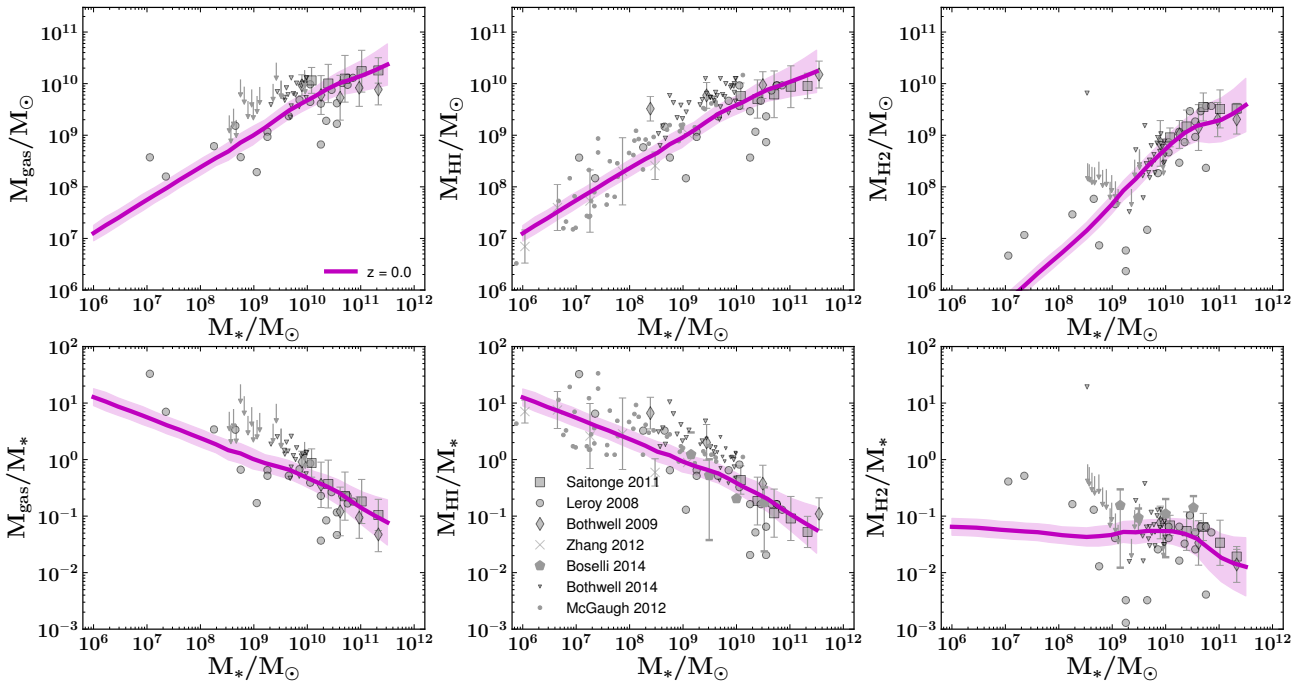


**Figure 3.** The cold gas mass (top left), H I mass (top row center column), $H_2$ mass (top right), gas-to-stellar mass ratio (bottom left), H I-to-stellar mass ratio (bottom row center column), and $H_2$-to-stellar mass ratio (bottom right) of galaxies as a function of stellar mass at $z = 0$. Shaded regions mark the one sigma of the posterior distribution of the inferred gas masses. Literature values are from Leroy et al. (2008), Bothwell, Kennicutt & Lee (2009), Saintonge et al. (2011), McGaugh (2012), Zhang et al. (2012), Boselli et al. (2014) and Bothwell et al. (2014) are shown in grey. Errorbars on the literature values mark the one-sigma distributions of the observed sample.

We show the redshift evolution of the cold gas, H I and $H_2$ mass and the cold gas-, H I- and $H_2$-to-stellar mass ratio of galaxies up to $z = 3$ in Figure 6. The shapes of the presented relations are roughly constant with time. The cold gas, H I, and $H_2$ mass of a galaxy increases and its gas-to-stellar mass and H I-to-stellar mass ratios decrease with stellar mass. The $H_2$-to-stellar mass ratio remains constant below stellar masses of $M_\star \sim 10^{10-10.5}\,M_\odot$ and decreases for galaxies with higher stellar masses, independent of redshift.

It is striking to see that as time evolves the normalization of the absolute and relative H I and $H_2$ contents of galaxies show very different behavior. We find very weak evolution in the H I content for galaxies with low stellar masses ($M_\star < 10^{9.5}\,M_\odot$). Galaxies with higher stellar masses show

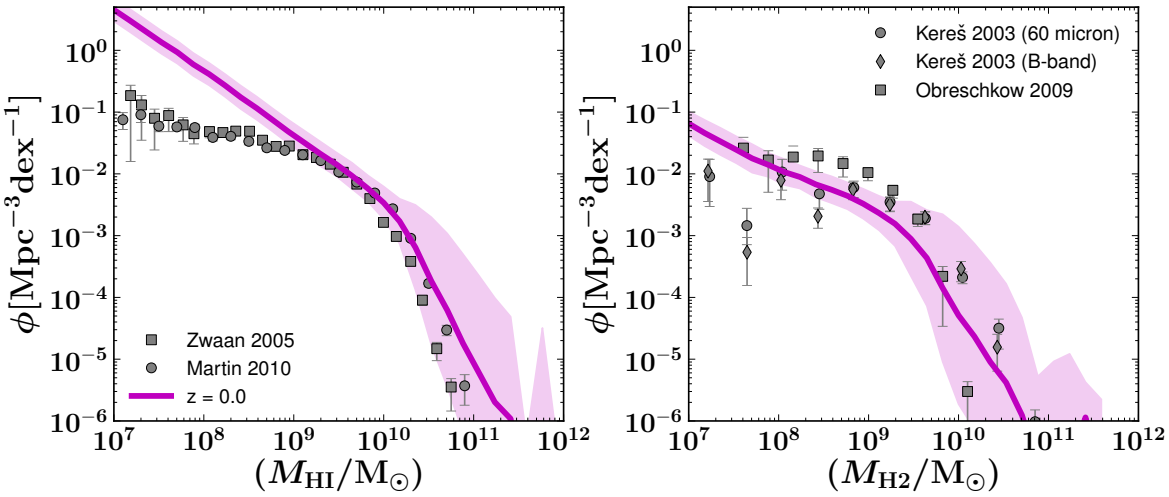


**Figure 4.** H I (left) and $H_2$ (right) mass function at $z = 0$. Model results are compared to literature results from Zwaan et al. (2005), and Martin et al. (2010) for H I and Kereš, Yun & Young (2003) and Obreschkow & Rawlings (2009) for $H_2$. The shaded regions show the one-sigma posterior distributions.

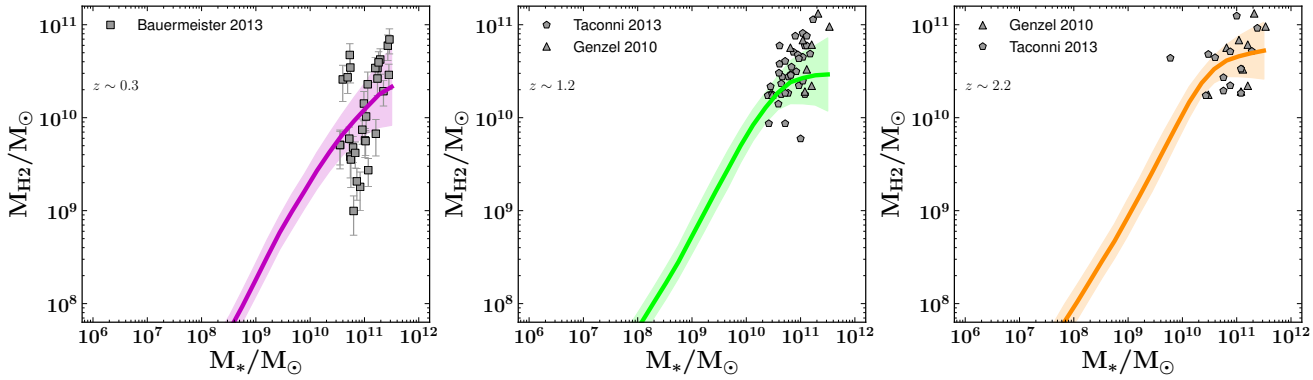


**Figure 5.** $H_2$ mass as a function of stellar mass at redshifts $z = 0.3$, $z = 1.2$, and $z = 2.2$. Shaded regions mark the one-sigma distributions of the inferred gas masses. Model results are compared to observations from Bauermeister et al. (2013) ($z = 0.3$), Tacconi et al. (2013) ($z = 1.2$ and $z = 2.2$), and the compilation presented in Genzel et al. (2010) ($z = 1.2$ and $z = 2.2$).

a much stronger evolution in their relative and absolute atomic gas mass. The H I mass of galaxies increases up to $z = 0.5$ and stays constant at later times. Below $z = 1$ the evolution in H I mass is less than a factor of three. We find very different evolution in the $H_2$ mass of galaxies with time. Galaxies at $z = 3$ have roughly ten times as much molecular hydrogen than local counterparts, independent of stellar mass and the strongest evolution in $H_2$ mass is at $z < 1$.

The relations between cold gas mass and gas-to-stellar mass ratios of galaxies and stellar mass are constant with time at $z < 0.5$. Only at later times does the total cold gas content of galaxies rapidly decrease.

### *3.2.2 H I and $H_2$ mass function*

We show the redshift evolution of the H I and $H_2$ mass functions up to redshift $z = 3$ in Figure 7. At fixed H I mass the number density of objects increases up to $z = 0.5$ and decreases at later times. At low H I masses ($M_{\rm HI} < 10^{9.5}\,{\rm M}_\odot$) the evolution in H I mass function with time is less than a factor three in number density at fixed H I mass. At higher masses the number density of objects rapidly increases up to $z = 2$, after which the evolution is weak. Only at $z < 0.5$ does the number density of galaxies with highest H I masses drop by an order of magnitude. The evolution in the H I mass function is in good agreement with predictions from semi-analytic models (e.g., Popping, Somerville & Trager 2014), but in poorer agreement with prediction using the hydrodynamical simulations presented in Davé et al. (2013) (we discuss this in Section 4). The steep slope in the low-mass end of the H I mass function as seen at $z = 0$ is present at all discussed redshifts. We discuss the origin of this steep slope in Section 4.5.

Our inferred $H_2$ mass function has the highest normalization at redshift $z \sim 2$. Largest $H_2$ reservoirs ($M_{\rm H2} \sim 10^{11.5-12}\,{\rm M}_\odot$) are also found at this redshift. These two results (highest number and most massive objects) coincide with the peak of the SFR density distribution of the Universe. The evolution in the $H_2$ mass function at redshifts

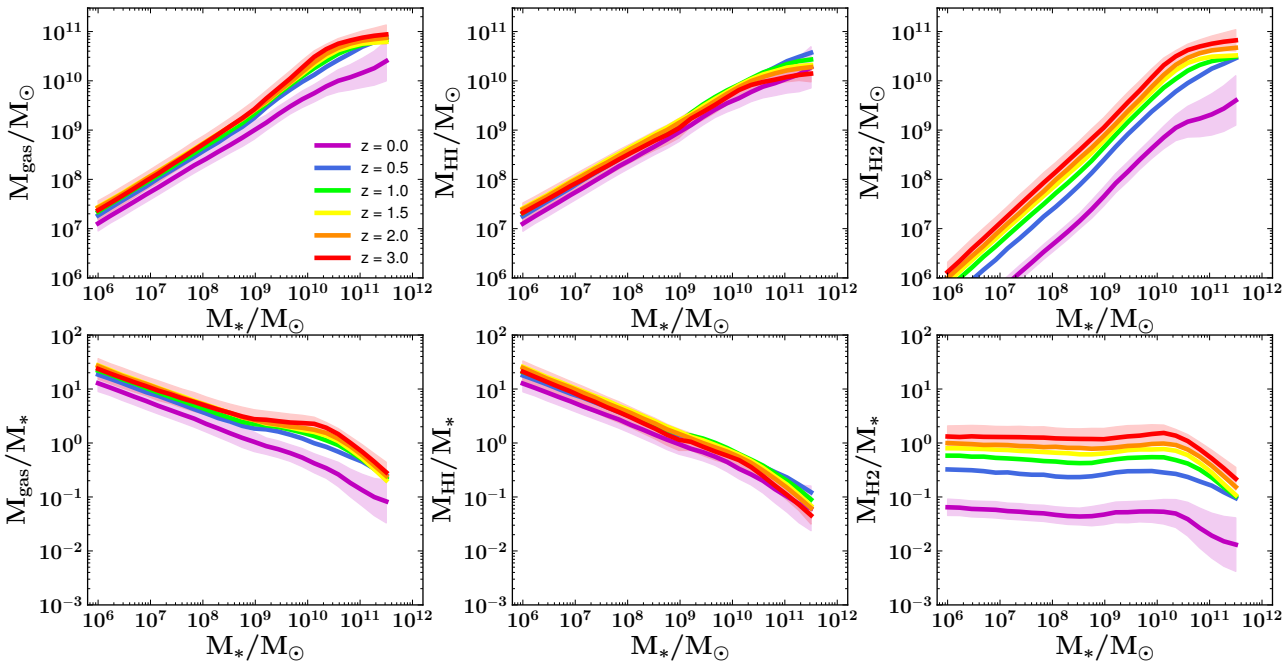


**Figure 6.** Redshift evolution of the cold gas mass (top left), H I mass (top row center column), $H_2$ mass (top right), gas-to-stellar mass ratio (bottom left), H I-to-stellar mass ratio (bottom row center column), and $H_2$-to-stellar mass ratio (bottom right) of galaxies as a function of stellar mass. Shaded regions mark the one-sigma posterior distributions of the inferred gas masses. For clarity we only show the one-sigma region at redshifts $z = 0$ and $z = 3$. The distribution at other redshifts is very similar.

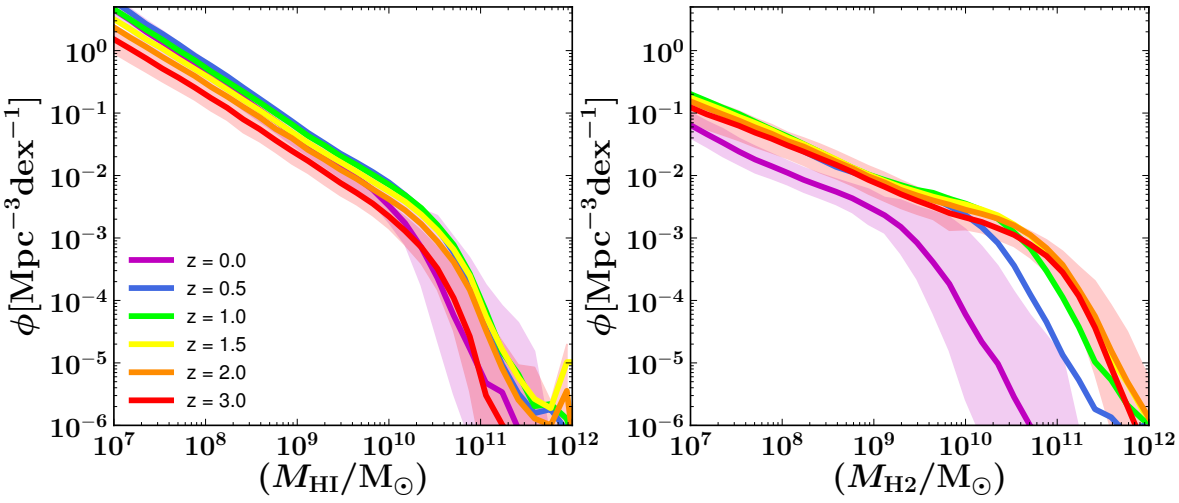


**Figure 7.** Evolution of the H I (left) and $H_2$ (right) mass functions with redshift. The shaded regions show the one-sigma posterior distributions. For clarity we only show the one-sigma region at redshifts $z = 0$ and $z = 3$. The distribution at other redshifts is very similar.

$1 < z < 3$ is weak. We find a much stronger evolution in the $H_2$ mass function at lower redshifts. The rapid decline in number density of galaxies with $M_{H2} > 10^{10}\,M_\odot$ starts at $z = 1$, whereas the decline in number density of less massive galaxies starts at $z < 0.5$. This suggests that galaxies with high $H_2$ masses lose their molecular gas at earlier times than less molecule rich galaxies.

It is intriguing to see that the evolution in the H I and $H_2$ mass functions do not go hand-in-hand. The strongest evolution in $H_2$ is observed at $z < 1$, where the cosmic SFR density is plummeting, whereas the H I mass function is much more constant in this redshift regime. Although the number of massive total (H I + $H_2$) cold gas reservoirs changes (especially at $z < 1$), this does not automatically mean that H I and $H_2$ independently follow the same trend.

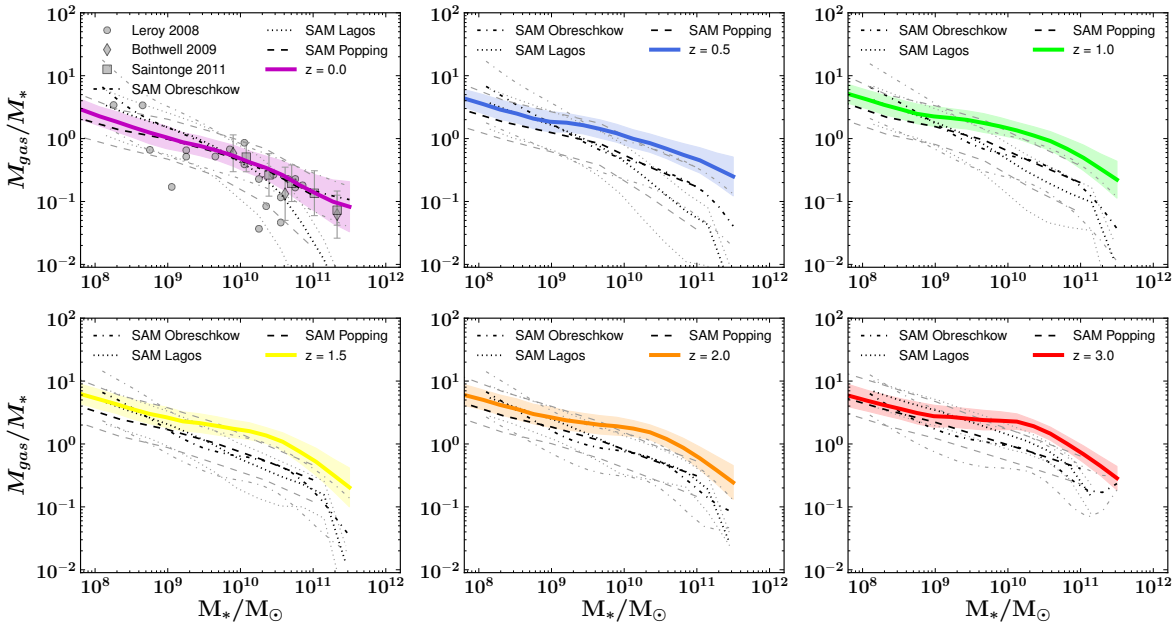


**Figure 8.** Gas fraction of galaxies as a function of stellar mass for different redshift bins. Shaded regions mark the one-sigma posterior distributions of the inferred gas fractions. Model results at $z = 0$ are compared to literature values from Leroy et al. (2008), Bothwell, Kennicutt & Lee (2009), and Saintonge et al. (2011). The black dashed, dotted, and dash-dotted lines represents the semi-analytic model predictions from Popping, Somerville & Trager (2014), Lagos et al. (2011), and Obreschkow et al. (2009).

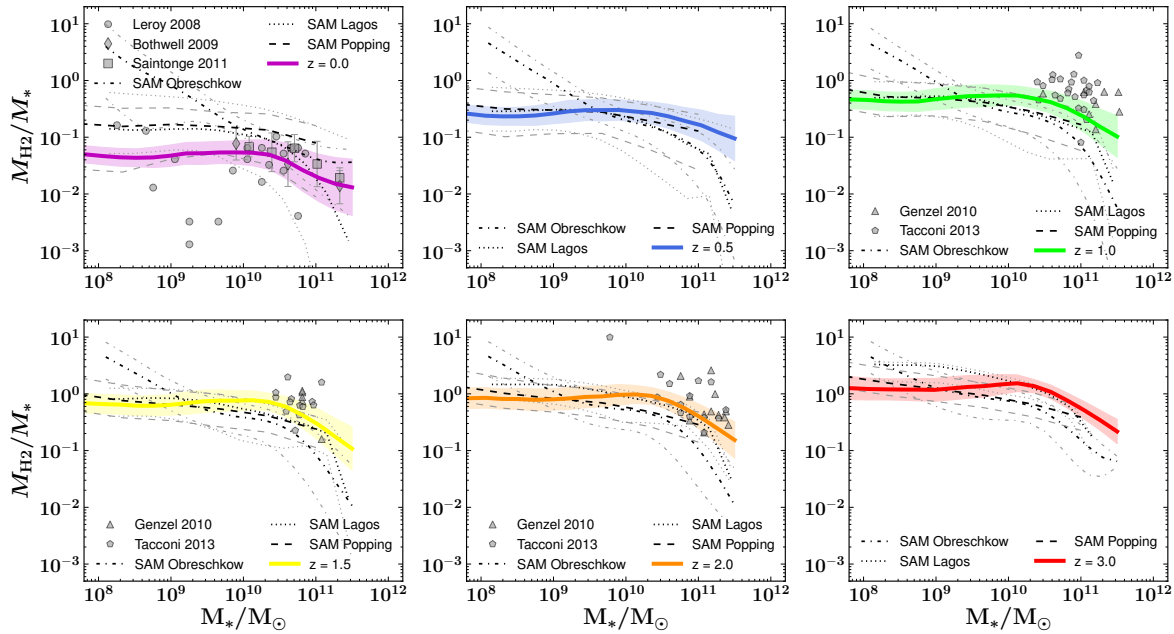


**Figure 9.** Relative $H_2$ content galaxies ($\frac{M_{H2}}{M_*}$) as a function of stellar mass for different redshift bins. Shaded regions mark the one-sigma posterior distributions of the inferred gas fractions. Model results are compared to literature values from Leroy et al. (2008),Bothwell, Kennicutt & Lee (2009), Genzel et al. (2010), Saintonge et al. (2011), and Tacconi et al. (2013). The black dashed, dotted, and dash-dotted lines represents the semi-analytic model predictions from Popping, Somerville & Trager (2014), Lagos et al. (2011), and Obreschkow et al. (2009).

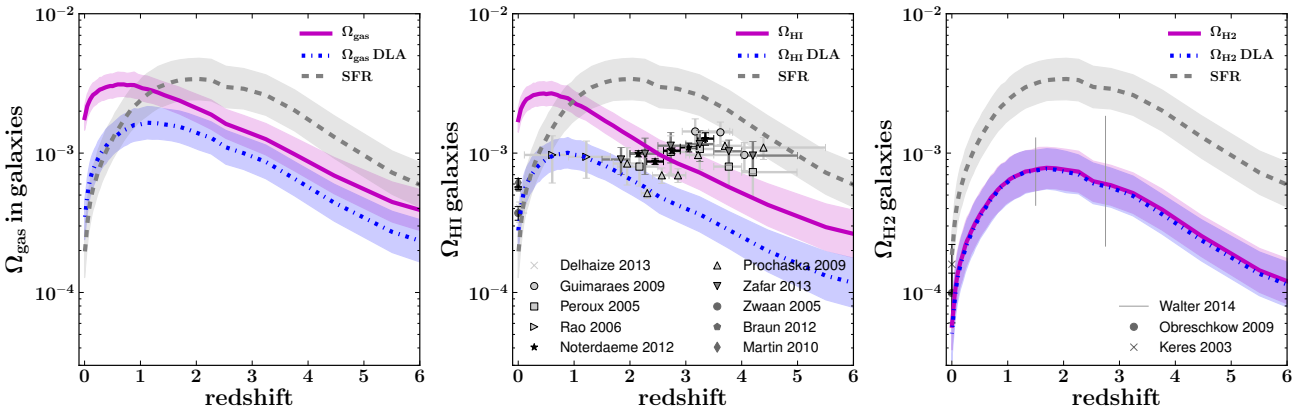


**Figure 10.** The cosmic comoving density, in units of the critical density, of cold gas (H I + $H_2$; top panel), H I (middle) and $H_2$ (bottom) as a function of redshift. Observations of Péroux et al. (2005), Rao, Turnshek & Nestor (2006), Guimarães et al. (2009), Prochaska & Wolfe (2009), Delhaize et al. (2013) are overplotted in light gray. Dark gray observations are by Zafar et al. (2013) and observations of local galaxies (Kereš, Yun & Young 2003; Zwaan et al. 2005; Martin et al. 2010; Obreschkow & Rawlings 2009; Braun 2012) are overplotted in black. Grey bars mark the observational constraint on $\Omega_{\rm H2}$ from Walter et al. (2014). The dotted grey line marks the evolution of the SFR density of the Universe in $\rm M_\odot\,yr^{-1}\,Mpc^{-3}$, scaled down by a factor of 50. The shaded regions show the one-sigma posterior distributions.

### *3.2.3 Galaxy gas fractions*

We present the gas fraction and relative $H_2$ content of galaxies as a function of stellar mass in Figures 8 and 9. Gas fractions are plotted at redshifts running from $z = 0$ to $z = 3$ and compared with direct observations and predictions based on the semi-analytic models by Obreschkow et al. (2009), Lagos et al. (2011), and Popping, Somerville & Trager (2014). The inferred gas masses can act as constraints for theoretical models and prescriptions that describe the baryonic cycle of matter within galaxies.

The cold gas fraction of a galaxy decreases with increasing stellar mass. At $z > 1$ we find a shallow slope in gas fraction for galaxies with $M_\star < 10^{10}\,\rm M_\odot$ followed by a rapid drop for galaxies with higher stellar masses. At lower redshifts galaxy gas fractions monotonically increase with stellar mass. The evolution in the normalization of galaxy gas fraction with time is weak. Most prominent evolution is found at stellar masses around $10^{10}\,\rm M_\odot$ and below $z = 0.5$.

The evolution in $\frac{\rm M_{H2}}{\rm M_\star}$ is much stronger than found for $f_{\rm gas}$ (Figure 9). At $z = 3$, $\frac{\rm M_{H2}}{\rm M_\star}$ reaches values of $\sim 2$, whereas it less than 0.1 at $z = 0$. Although at $z = 0$ low-stellar mass galaxies are dominated by their cold gas content, the $H_2$ fraction of this gas is very low. At $z = 3$, on the other hand, most of the cold gas is molecular. We find a peak in $\frac{\rm M_{H2}}{\rm M_\star}$ for galaxies with stellar masses near $10^{10}\,\rm M_\odot$ at all redshifts. There is a minor increase with stellar mass below this characteristic mass, whereas we find a rapid drop in $\frac{\rm M_{H2}}{\rm M_\star}$ above this characteristic mass. This suggests galaxies are most efficient in forming $H_2$ and transforming cold gas into stars near $M_\star = 10^{10}\,\rm M_\odot$. We will explore which haloes host these galaxies and what light this sheds on the stellar build-up of galaxies in Section 3.3.

We compare our findings for $\frac{\rm M_{H2}}{\rm M_\star}$ to literature values presented in Tacconi et al. (2013) and the compilation from Genzel et al. (2010) (obtained through CO). Direct observations of $\frac{\rm M_{H2}}{\rm M_\star}$ are within the scatter of our inferred $H_2$ masses, although at the high side compared to our mean trends. We ascribe this to the strongly biased nature of the observations at these redshifts towards actively star-forming (and therefore $H_2$ rich) galaxies. Nevertheless the rough agreement between observations and our results for these stellar massive galaxies is very encouraging.

The presented trends provide constraints for theoretical models including a detailed prescription for galaxy cold gas content. These constraints have the potential to break degeneracies between different physical recipes included in models. Unlike indirect gas estimates from large optical surveys (Popping et al. 2012, Popping et al. in prep.), the work presented here is not biased by selection criteria and represents a complete sample. Semi-analytic model predicts a similar shape in the trend between gas fractions and $\frac{\rm M_{H2}}{\rm M_\star}$ with stellar mass and with redshift as our semi-empirical model. The normalization of the trends at $M_\star > 10^{10}\,\rm M_\odot$ predicted by semi-analytic models at $z \geqslant 0.5$ is systematically below the results presented in this work. The discrepancy is especially obvious in the gas fractions in the redshift regime $1 < z < 2.5$. This suggests that in semi-analytic models galaxies have expelled and/or consumed more of their cold gas. A similar dearth of molecular hydrogen in this redshift regime was found in a comparison between semi-analytic model predictions and indirect $H_2$ estimates taken from the COSMOS sample (Lu et al. 2014a; Popping, Somerville & Trager 2014; White, Somerville & Ferguson 2014). This is likely coupled to the low-mass galaxy problem, where galaxies in theoretical models form their stars and consume their gas too early.

### *3.2.4 Cosmic gas density in galaxies*

We present our inferences for the total cold gas (H I + $H_2$), H I, and $H_2$ cosmic density of the Universe as a function of time in Figure 10. We compare our results to local H I and $H_2$ densities (Kereš, Yun & Young 2003; Zwaan et al. 2005; Obreschkow & Rawlings 2009; Martin et al. 2010; Braun

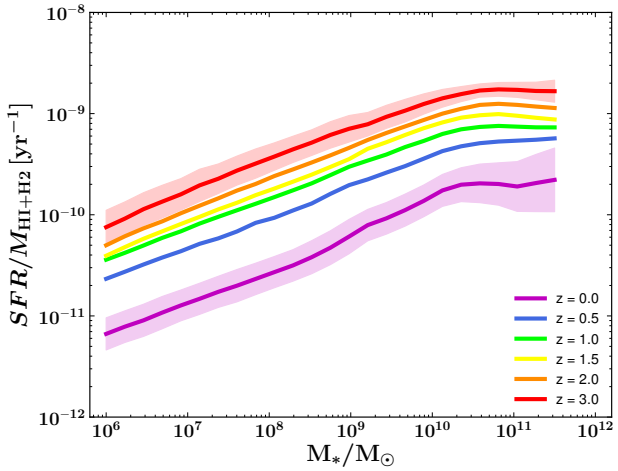


**Figure 11.** Redshift evolution of the star-formation efficiency (SFE $\equiv$ SFR/$M_{HI+H2}$) of galaxies as a function of stellar mass. Solid lines mark the mean trends and shaded colors mark the one-sigma distribution of the inferred gas masses. For clarity we only show the one-sigma regions at redshifts $z = 0$ and $z = 3$. The distribution at other redshifts is very similar.

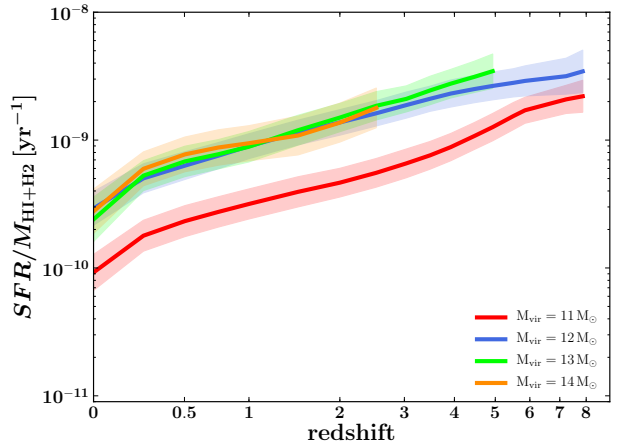


**Figure 12.** The star-formation efficiency (SFE $\equiv$ SFR/$M_{HI+H2}$) of galaxies as a function of redshift in different halo mass bins. Shaded regions mark the one-sigma distributions of the star-formation efficiencies.

2012) and higher redshift estimates of the $H_2$ (Walter et al. 2014) and H I density obtained through stacking (Delhaize et al. 2013) and from DLAs (e.g., Péroux et al. 2005; Rao, Turnshek & Nestor 2006; Guimarães et al. 2009; Prochaska & Wolfe 2009; Zafar et al. 2013).

We find a gradual increase in the total cold gas cosmic density with redshifts up to $z \sim 1$ followed by a rapid drop at lower redshifts. A similar trend is found for the H I cosmic density, which peaks at $z \sim 0.5$. The evolution in $\Omega_{HI}$ is relatively weak in the redshift regime $0 < z < 2$. The $H_2$ cosmic density on the other hand increases gradually up to $z \sim 1.5$ and shows a rapid drop at lower redshifts, closely following the evolution of the cosmic SFR. The inferred $H_2$ cosmic density of gas in galaxies never exceeds the H I cosmic density.

We reach good agreement with the constraints on $\Omega_{H2}$ at redshifts $z = 1.5$ and $z = 2.75$ (Walter et al. 2014), supporting an increase in the cosmic $H_2$ density. The observational constraints are unfortunately not tight enough to separate between a peak, a flat, or declining evolution in $\Omega_{H2}$ at $z > 2$. Our approach overpredicts the observational estimates of $\Omega_{HI}$ at $z < 2$ and underpredicts $\Omega_{HI}$ at redshifts $z > 3$. In the low redshift regime this is due to the high number of galaxies with low H I masses, in poor agreement with the observed H I mass function at $z = 0$. We warn the reader that in this work we only probe the cold gas that is associated to the galaxy disc (down to a hydrogen column density of $N_H = 10^{18}\,\mathrm{cm}^{-2}$), ignoring DLAs that may arise from intergalactic gas in cold streams or filaments at $z > 1.5 - 2$ (Berry et al. 2014). As a comparison we include inferred cosmic densities when only taking gas above the DLA column density into account (i.e. $N_H > 2 \times 10^{20}\,\mathrm{cm}^{-2}$). The resulting cosmic densities for cold gas and H I decrease by a factor of $\sim 4$, whereas this selection does not affect the $H_2$ cosmic density. Our predictions for the H I cosmic densities are now in good agreement with observations out to $z \approx 2$, but at higher redshifts our inferred cosmic H I densities are lower than the observed densities.

#### *3.2.5 Star-formation efficiency*

The star-formation efficiency (here defined as SFE $\equiv$ SFR/$M_{HI+H2}$) measures the ability of a galaxy to transform cold gas into stars.[2] We present the SFE of galaxies as a function of stellar mass and redshift in Figure 11. The SFE of galaxies increases with stellar mass, independent of redshift. Although the relative gas content of galaxies decreases with stellar mass (Figure 8), the ability of the gas to form stars increases. This is largely set by a decrease in the H I content of galaxies with increasing stellar mass. At fixed stellar mass, the SFE of galaxies decreases with time, resembling the evolution of the $H_2$ content of galaxies (Figure 6; note, however, that in our model the $H_2$ mass of a galaxy is largely controlled by its SFR).

There is a plateau in the SFE of galaxies at stellar masses $M_\star > 10^{10}\,M_\odot$, independent of redshift. At fixed redshift, star-forming galaxies have reached their maximum SFE at this characteristic stellar mass. It is at the same characteristic stellar mass that the relative $H_2$ content of galaxies, $\frac{M_{H2}}{M_\star}$, rapidly drops. We find a similar constancy in the SFE of galaxies as a function of their redshift in different bins of halo mass (Figure 12). At fixed redshift the SFE of star-forming galaxies is constant as a function of halo mass for galaxies residing in haloes more massive than $10^{12}\,M_\odot$. The SFE of galaxies decreases with time for a fixed host halo mass. The constancy of SFE at fixed redshift is in agreement with the plateau in SFE we found for galaxies with stellar masses larger than $10^{10}\,M_\odot$.

### 3.3 Cold gas content of dark matter haloes

In this section we present the gas content of galaxies as a function of their host halo mass. We warn the reader that

[2] This is different from a commonly used definition for star-formation efficiency; the fragment of gas mass converted into stars

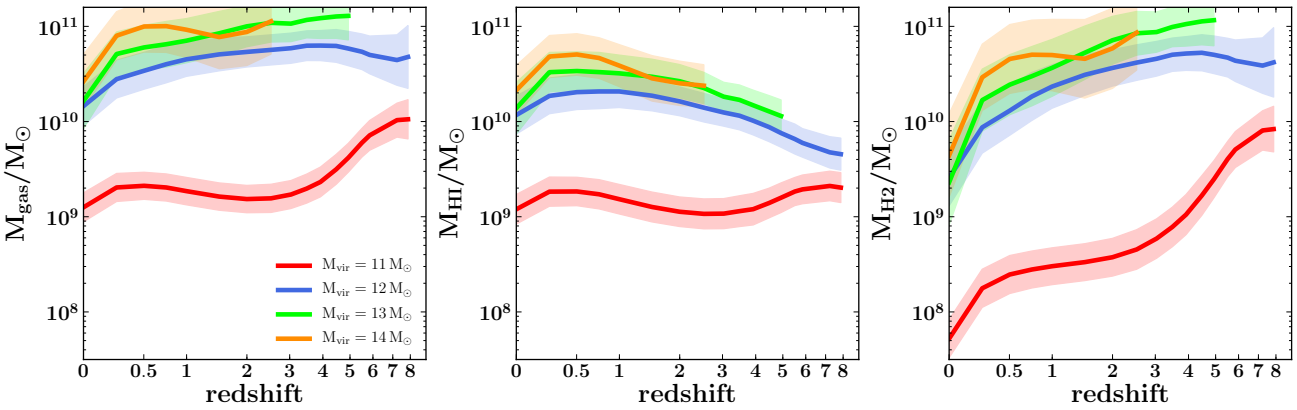


**Figure 13.** Average cold gas mass (H I + $H_2$; left panel), H I mass (middle panel), and $H_2$ mass (right panel) as a function of redshift for galaxies in haloes at fixed halo mass. Shaded regions mark the one-sigma posterior distributions of the inferred gas masses.

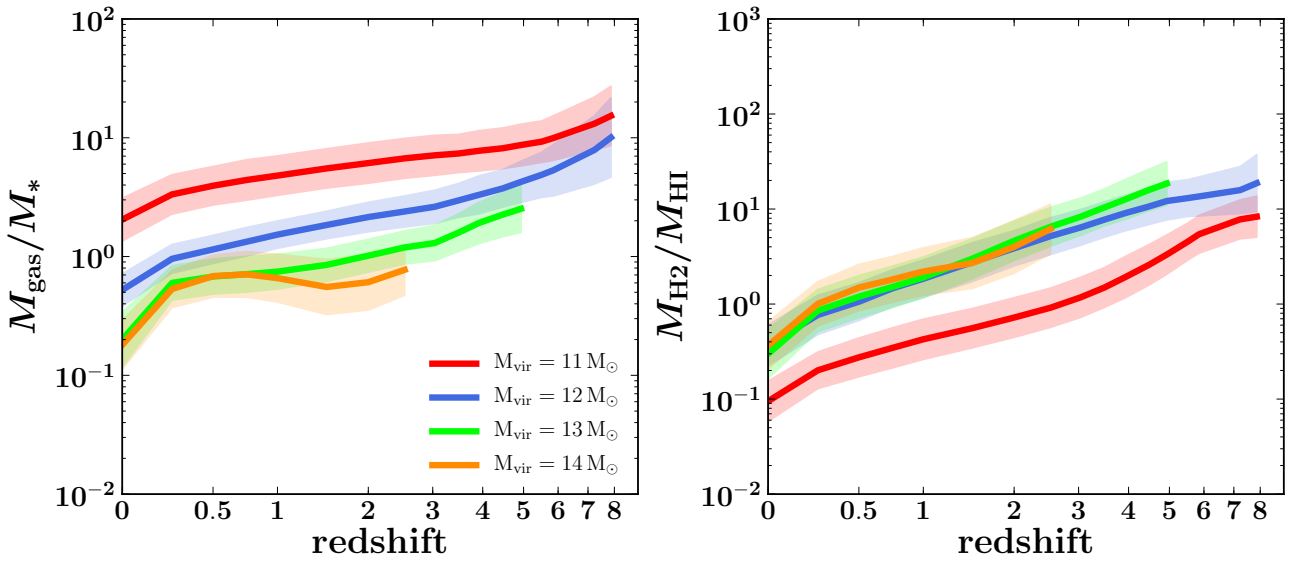


**Figure 14.** Cold gas-to-stellar mass ratio (left) and $H_2$-to-H I mass ratio (right) of galaxies as a function of redshift in different halo mass bins. Shaded regions mark the one-sigma posterior distributions of the inferred gas masses.

we only infer gas masses for star-forming galaxies and do not account for cold gas in early-type galaxies.

We show derived cold gas, H I, and $H_2$ masses as a function of halo mass and redshift in Figure 13. We find that the evolution of the total cold gas content of galaxies is very different as a function of their host halo mass. The gas content of galaxies residing in haloes with $M_h = 10^{14}\,M_\odot$ increases up to $z = 0.5$ after which it rapidly decreases. Less massive haloes show a weak decrease in their cold gas content with time. The gas content of galaxies residing in haloes with mass $M_h = 10^{11}\,M_\odot$ rapidly decreases with time until $z \sim 3$, after which it stays relatively constant.

Much stronger evolution is found for the H I and $H_2$ mass of galaxies. Independent of halo mass the H I mass increases with time up to $z \sim 0.5$ and decreases at lower redshifts. The most rapid increase in atomic gas mass is found for galaxies residing in haloes with masses larger than $10^{12}\,M_\odot$. We find a decrease in the $H_2$ mass of galaxies at all redshifts. For galaxies residing in haloes with masses $M_{vir} \geqslant 10^{12}\,M_\odot$ most rapid decrease is found at redshifts $z < 1$. For galaxies residing in less massive haloes the decrease in $H_2$ mass is most rapid at $z > 2$ and $z < 0.5$.

We find minor differences in the absolute amount of cold gas, H I and $H_2$ in haloes more massive than $M_h = 10^{12}\,M_\odot$. Although in the most massive haloes many more baryons are potentially available to cool down onto their central galaxy, these objects have only twice as large cold gas reservoirs than other galaxies. The physical processes acting on the cold gas prevent galaxies to build up gas reservoirs much larger than on average a few times $10^{10}$ solar masses.

In Figure 14 we show the relative gas and $H_2$ content of galaxies as a function of time at fixed halo mass. Galaxies residing in low-mass haloes ($10^{11}\,M_\odot$) are dominated by their cold gas content. There is only weak evolution in the gas-to-stellar mass ratio for these galaxies. We find a gradual decrease in relative cold gas content with time for more

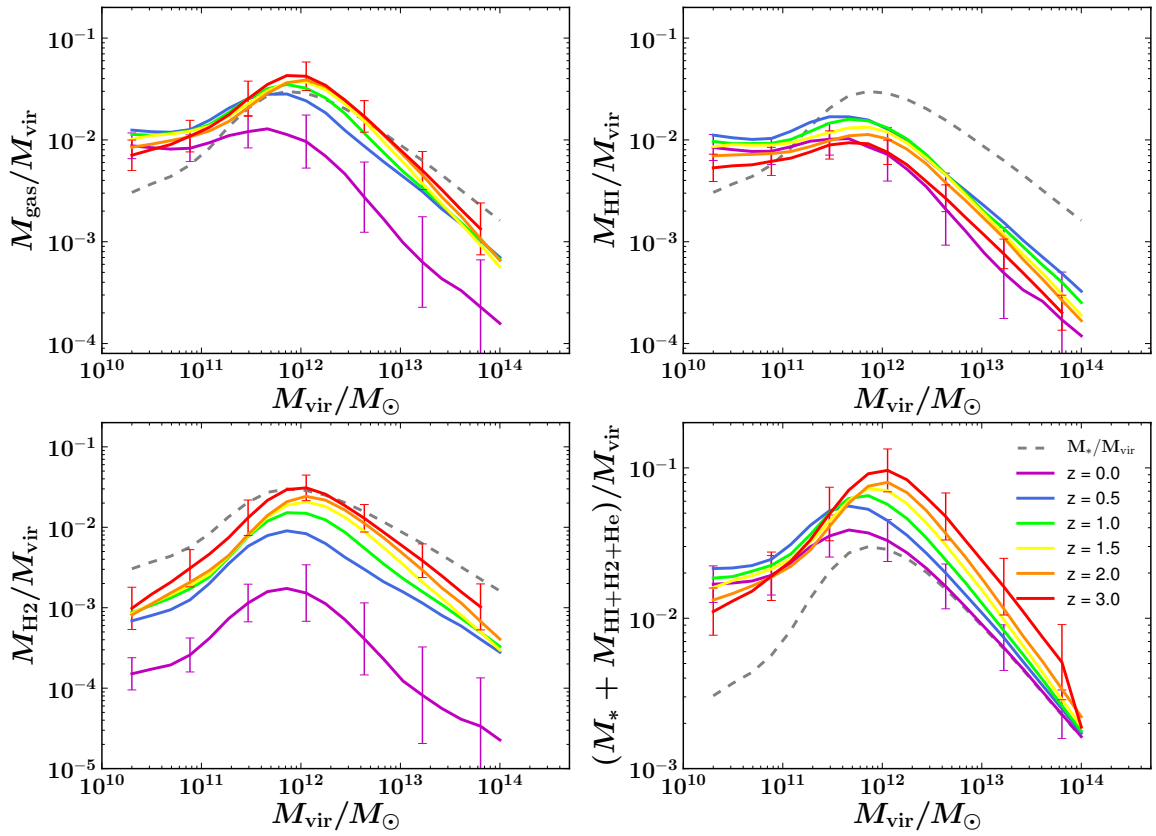


**Figure 15.** Relative cold gas content (H I + $H_2$; upper left panel), H I content (upper right panel), $H_2$ content (lower left panel), and combined gas and stellar content including Helium (lower right panel) as a function of halo mass for different redshift bins. Errorbars mark the one-sigma posterior distributions of the inferred gas masses. The dotted grey line marks the stellar-to-halo mass ratio ($M_\star/M_{\rm vir}$) of galaxies at $z = 0$.

massive haloes. We find a minor increase in cold gas content until $z = 0.5$ followed by a decline for the most massive haloes probed. Independent of host halo mass the relative $H_2$ fraction of the cold gas in galaxies decreases rapidly with time. At $z > 3$ nearly all the cold gas in haloes is molecular, whereas at $z = 0$ it is less than 25 percent. The relative $H_2$ fraction is almost constant for haloes with masses of $M_{\rm h} \geqslant 10^{12}\,{\rm M}_\odot$. Despite the cold gas reservoir being relatively smaller for the highest mass haloes, this does not affect the ability of the cold gas to form molecules.

We show the ratio of cold gas, H I, $H_2$, and total baryonic content in the disc ($M_\star + M_{\rm HI} + M_{\rm H2}$; including a 1.36 contribution for Helium) with halo mass as a function of halo mass at different redshifts in Figure 15. These ratios provide insight into the fraction of baryons stored in cold gas and/or stars in the disc of central galaxies and the relative amount of baryons in haloes that may participate in the formation of stars.

There is a peak in the gas-to-halo mass (H I and $H_2$ combined) and in the $H_2$-to-halo mass ratio around $M_{\rm vir} = 10^{12}\,{\rm M}_\odot$ at all redshifts. The exact location of this characteristic halo mass moves towards higher masses with increasing redshift, resembling the characteristic halo mass at which the stellar-to-halo mass ratio peaks (Behroozi, Wechsler & Conroy 2013b). Below $M_{\rm vir} = 10^{12}\,{\rm M}_\odot$ the slope of the $H_2$-to-halo mass ratio is much steeper than it is for the H I-to-halo mass ratio (and cold gas mass). The drop in gas-to-halo mass ratio for haloes more massive than $10^{12}\,{\rm M}_\odot$ is similar for atomic and molecular hydrogen. The strong peak in the $H_2$-to-halo mass ratio suggests that there is a favorable range of halo masses at which galaxies host relatively largest molecular gas reservoirs out of which new stars may form.

The normalization of the different relations presented in Figure 15 changes strongly with redshift. The relative cold gas content of a halo decreases by approximately a factor of three from $z = 3$ to $z = 0$. The relative H I content of a halo grows up to $z = 0.5$ and mildly decreases at lower redshift. The relative $H_2$ content of a halo is highest at $z = 3$ and decreases by more than a full order of magnitude afterwards.

We present the total baryonic content (stars combined with H I and $H_2$) in the central galaxy of a halo in the bottom-right panel of Figure 15. At $z = 0$ the ratio between the total baryonic mass in the galaxy and the halo mass peaks at $M_{\rm vir} \approx 3 \times 10^{11}\,{\rm M}_\odot$. This peak moves towards higher masses with increasing redshift. The absolute value in the peak of the fraction of baryons of a halo that are stored in the galaxy decreases from $z = 3$ to $z = 0$ by less than half a dex. Only in low mass haloes with masses of a few times $10^{11}$ solar masses and less does the baryonic content of a halo stored in the central galaxy peak at $z = 0.5$, driven by large H I reservoirs. There is no evolution in the baryonic

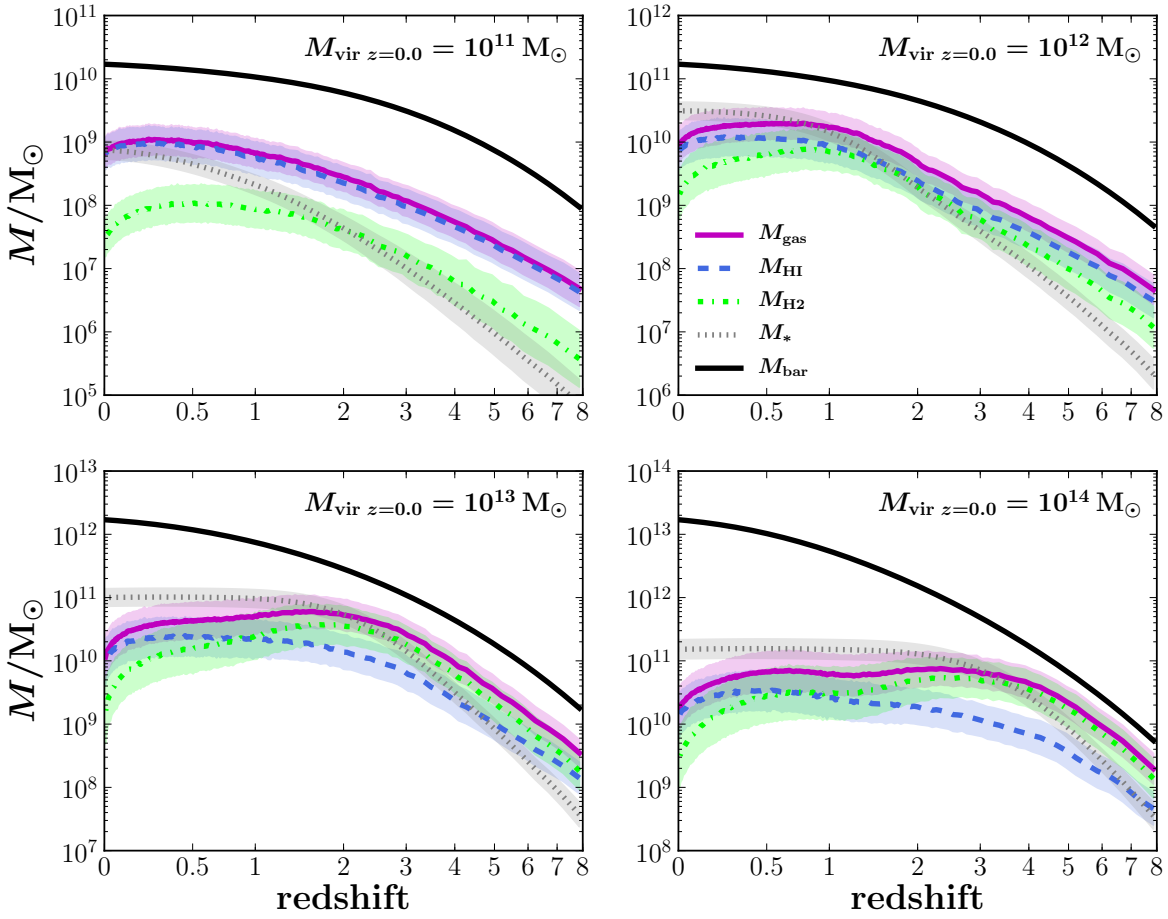


**Figure 16.** Time evolution of the total cold gas (solid purple), H I (dashed blue), $H_2$ (dashed dotted green), stellar (dashed grey) and mass of baryons in the halo (solid black) for haloes as a function of their $z = 0$ halo mass for the median mass accretion history. The shaded regions show the one-sigma posterior distributions.

mass ratio for galaxies residing in haloes more massive than $10^{13}\,{\rm M}_\odot$. Galaxies in these haloes have low gas fractions and are dominated by their stellar content.

Haloes with masses of a few times $10^{11}$ solar masses are most efficient stroring their baryons in stars and cold gas within the central galaxy. At $z = 3$ roughly 30 percent of the available baryons are locked up in stars and cold gas in the central galaxy. At $z = 0$ this number decreased to roughly 17 percent. The ability of haloes to store their baryons in stars and cold gas is poorer at lower and higher halo masses. These results suggest that the low baryon conversion efficiency of haloes is driven by the inability of haloes to build large gas reservoirs in galaxy discs.

We present the time evolution of the total cold gas content and H I and $H_2$ mass of galaxies as a function of their $z = 0$ halo mass in Figure 16. For massive haloes ($M_{\rm vir} \geqslant 10^{13}\,{\rm M}_\odot$) the cold gas content increases until the haloes have reached a baryonic mass of approximately 3–$4 \times 10^{11}\,{\rm M}_\odot$ (which translates to a virial mass of roughly $10^{12}\,{\rm M}_\odot$). At lower redshifts the cold gas content of galaxies decreases gradually. Although the gas content of central galaxies decreases, the baryonic content of the halo keeps growing. For less massive haloes the cold gas content increases up to $z = 1$ ($M_{\rm vir\ z=0} = 10^{12}\,{\rm M}_\odot$) or even until almost present day ($M_{\rm vir\ z=0} = 10^{11}\,{\rm M}_\odot$).

A close inspection reveals that the baryonic mass of the host halo at the time that the galaxies have gained largest gas reservoir increases with more than an order of magnitude with increasing $z = 0$ halo mass ($1.5 \times 10^{10}\,{\rm M}_\odot$ for $M_{\rm vir\ z=0} = 10^{11}\,{\rm M}_\odot$ and $5.7 \times 10^{11}\,{\rm M}_\odot$ for $M_{\rm vir\ z=0} = 10^{14}\,{\rm M}_\odot$). Furthermore, the gas content increases more rapidly in galaxies that end up in massive haloes ($M_{\rm vir\ z=0} > 10^{13}\,{\rm M}_\odot$) than in galaxies that end up in less massive haloes. The increase in cold gas mass before a galaxy reaches its peak gas mass is steeper than the decrease afterwards. The peak in the total cold gas content coincides with a flattening in the stellar buildup of star-forming galaxies. The redshift at which the stellar mass dominates of the gas mass in a galaxies decreases with decreasing $z = 0$ host halo mass.

We clearly see that the evolution in the H I and $H_2$ content of galaxies changes with $z = 0$ host halo mass as well. The cold gas is always dominated by atomic hydrogen in galaxies residing in haloes with $M_{\rm vir\ z=0} \leqslant 10^{12}\,{\rm M}_\odot$. The dominance of H I decreases as a function of $z = 0$ host halo mass. For galaxies residing more massive $z = 0$ haloes the cold gas is first mostly molecular and only at later times

does the atomic hydrogen dominate. The transition from an atomic to a molecular dominated interstellar medium occurs at $z \sim 1$–$1.5$, after the peak in cold gas content of galaxies. Figure 16 also shows that the evolution in H I mass at $z < 1.5$ of galaxies is very minor, whereas the $H_2$ mass decreases by at least an order of magnitude. Independent of halo mass the fraction of baryons *n*ot stored in the central galaxy increases rapidly once the host halo reached a mass of $\sim 10^{12}\,\mathrm{M}_\odot$.

## 4 DISCUSSION

We have combined an abundance modeling approach (Behroozi, Wechsler & Conroy 2013b) with a method to indirectly estimate galaxy gas masses (Popping et al. 2012) to infer the cold gas content of galaxies as a function of time and halo mass. It has the unique capacity to obtain data-driven inferences of the H I and $H_2$ mass of galaxies and couple these to galaxy host halo mass.

### 4.1 Mild evolution in the H I mass of galaxies

Our results suggest mild evolution in the H I content of galaxies at fixed stellar mass, whereas the $H_2$ content decreases rapidly. This picture is supported by the evolution of the H I and $H_2$ mass function. The $H_2$ mass function shows a strong evolution of more than a dex with time (especially in the redshift range $z = 1 - 0$), whereas the H I mass function is fairly constant at $z < 2$ (although note the drop in the normalization of the H I mass function at $z < 0.5$ for galaxies with H I masses larger than $10^{10}\,\mathrm{M}_\odot$). Furthermore, we find very minor evolution in the H I mass of galaxies at $z < 1.5$ as a function of their $z = 0$ host halo mass. Within our model, the $H_2$ content of a galaxy is, to first order, controlled by the SFR (Equation 2). The H I content of a galaxy is controlled by the amount of cold gas available, combined with its partitioning into atoms and molecules. This partitioning is set by the amount of gas necessary to provide the pressure to support the formation of $H_2$ out of which stars may form. The relatively weak evolution in galaxy H I content and the H I mass function is the result of a self-regulated equilibrium that arises naturally in galaxies. This equilibrium marks the balance between the available cold gas content and the transformation of H I into $H_2$. Observations have shown that atomic hydrogen saturates at surface densities of $\Sigma_{\mathrm{HI}} = 6 - 10\,\mathrm{M}_\odot\,\mathrm{pc}^{-2}$ and that cold gas at higher densities is dominated by molecular hydrogen (Blitz & Rosolowsky 2006; Leroy et al. 2008). As the cold gas content and surface density of galaxies decreases due to gas consumption and disc growth, the amount of cold gas that is locked up in molecular hydrogen also rapidly decreases. This process may prevent a rapid drop in the H I reservoir of galaxies but does not imply the weak evolution we find. It is the rate at which galaxies loose their cold gas (through SF and/or feedback) and their discs grow that sets the $H_2$ fraction of the cold gas and the weak evolution in galaxy H I content. This provides an interesting constraint for theoretical models that include the partitioning of cold gas into H I and $H_2$.

Popping, Somerville & Trager (2014) found a similar evolution in the normalization and slope of the H I mass function at $z < 2$. They used various $H_2$ formation recipes in their semi-analytical model, among which the same as employed in this work. Popping et al. also overpredict the number density of galaxies with low H I masses ($M_{HI} < 10^9\,\mathrm{M}_\odot$), although not as dramatically as in Figure 4 and ascribe the excess of galaxies with low H I masses to the inefficient conversion of atomic into molecular hydrogen in low mass haloes ($M_{\mathrm{vir}} < 10^{10}\,\mathrm{M}_\odot$). Other semi-analytic approaches reached similar conclusions (Obreschkow et al. 2009; Lagos et al. 2011; Fu et al. 2012). Using a hydrodynamic code, Davé et al. (2013) found a strong evolution in the slope of the low-mass end of the H I mass function, unlike the results presented in this work. Davé et al. use the same recipe to separate the atomic from the molecular gas as we us here. The authors find that the evolution in the low-mass-end of the H I mass function directly follows the evolution of the stellar mass function, due to a constant ratio between the H I and the stellar mass of galaxies.

### 4.2 Galaxy gas fractions

The cold gas fraction of a galaxy is set by the competition between the accretion, heating, outflow, and the consumption of cold gas by star formation (Tinsley 1980; Davé, Finlator & Oppenheimer 2011). The evolutionary trend of cold gas fractions with time therefore provides a unique insight into the importance of each of these processes. We find that the cold gas fractions of galaxies decrease at $z < 3$ with the most rapid decrease found at $z < 1.5$. This suggests that the accretion of gas onto galaxies cannot cope with the consumption and/or outflow of gas. Cosmological hydrodynamical simulations predict a decline in their 'cold mode' accretion rates onto galaxies at $z < 2$ (Birnboim & Dekel 2003; Kereš et al. 2005, 2009; Dekel & Birnboim 2006; Dekel et al. 2009). The decrease in cold gas fraction at $z < 1.5$ is in good agreement with a lack of accretion of new cold material onto galaxies. This supports a picture in which below $z = 2$ the infalling gas is sparse enough to be heated up or blown away by shock heating or feedback from an active galactic nucleus (though see Oppenheimer et al. 2010).

We have seen that $\frac{\mathrm{M_{H2}}}{\mathrm{M_\star}}$ evolves much more quickly than the combined H I +$H_2$ fraction of galaxies. The evolution of the atomic and molecular gas mass of a galaxy do not necessarily go hand-in-hand. The process that suppresses the formation of stars is at least two-fold: galaxies have lower cold gas fractions and lower molecular fractions. This was also found in other efforts to indirectly infer the gas mass of galaxies (Popping et al. 2012, Popping et al. in prep.). Previous efforts were always based on a biased sample, whereas our semi-empirical approach is unbiased. This conclusion is supported by the decline in SFE with time at fixed stellar mass. Not only the available gas reservoirs decrease, but the ability of the cold gas to form stars also decreases.

We have found that galaxies with the highest stellar masses run out of cold gas well before the lowest mass galaxies. This behavior is also prominent in the evolution of $\frac{\mathrm{M_{H2}}}{\mathrm{M_\star}}$ with stellar mass and time. Popping et al. (2012) and Popping et al. (in prep.) found the same trend when looking at the indirectly estimated gas content of galaxies taken from the COSMOS (Scoville et al. 2007) and CANDELS (Grogin et al. 2011; Koekemoer et al. 2011) surveys. Popping et al. (2012) referred to this trend as a different manifestation of downsizing in SF, which can be described as the de-

cline in mass for star-forming galaxies with increasing time (Fontanot et al. 2009). This behavior is supported by the evolution of the $H_2$ mass function: the number density of galaxies with high $H_2$ masses decreases at earlier times than the number density of galaxies with low $H_2$ masses. This suggests that downsizing may be linked to the evolution of the molecular gas content of galaxies.

Theoretical models predict a similar evolution for $f_{\rm gas}$ and $\frac{\rm M_{H2}}{\rm M_\star}$, although the normalization of the gas fraction with time is lower. Models are known to form their stars too early (especially in galaxies with low stellar mass, Weinmann et al. 2012) and the low gas fractions may be a reflection of the same physical process that drives the low-mass galaxy problem (White, Somerville & Ferguson 2014). Our results have the potential to act as a constraint on the physical recipes included in models acting on the cold gas content of galaxies. White, Somerville & Ferguson (2014) present the "parking-lot" picture as a potential solution to the low-mass galaxy problem. In this picture, when a halo accretes a smaller halo, the reservoir of ejected gas from the minor progenitor is added to the reservoir of the ejected gas of the new resulting halo (rather than adding it to the hot gas reservoir as was previously done in semi-analytic models). The model then adopts various scaling relations for the time after which the gas parked in this reservoir of ejected gas can accrete into the halo and cool onto the galaxy. This gas cools down and participates in the formation of stars at a later time when adopting the "parking-lot" picture than in the previous versions of the semi-analytic model. White, Somerville & Ferguson (2014) showed that this process increases the predicted gas fractions of galaxies at our redshifts of interest, in better agreement with our inferred gas fractions.

### 4.3 Cosmic densities

We obtain good agreement with the observed values for the cosmic H I density at $z \approx 2$–$3$ and correctly reproduce the observational constraints on the cosmic $H_2$ density at redshifts $z = 1.5$ and $z = 2.75$. The relatively constant evolution in $\Omega_{\rm HI}$ at $z < 2$ is in sharp contrast with the evolution of the cosmic star-formation rate, whereas the molecular hydrogen density (by construction) tightly follows the SFR density and decreases by over an order of magnitude in the same redshift regime. This suggests that in a model where the SFR of a galaxy is controlled by the available molecular gas, one can simultaneously reproduce the peak in cosmic SFR and the weak evolution of the H I density of the Universe during the same cosmic epoch. A similar conclusions was reached using theoretical models (Obreschkow et al. 2009; Bauermeister, Blitz & Ma 2010; Lagos et al. 2011; Popping, Somerville & Trager 2014), but this has not been addressed before through a data-driven approach as presented in this work.

### 4.4 On the gas properties that drive the peak in the stellar mass - halo mass ratio

Abundance matching approaches have demonstrated the importance of the galaxy-halo connection. Haloes near $10^{12}\,{\rm M}_\odot$ are most efficient turning their baryons into stars (Behroozi, Wechsler & Conroy 2013a). This maximum efficiency is supported by the gas content of galaxies. Haloes with masses near the characteristic mass of $10^{12}\,{\rm M}_\odot$ have the highest gas-to-halo mass ratio. The $H_2$-to-halo mass ratio shows an especially strong peak near $10^{12}\,{\rm M}_\odot$. This is not necessarily due to small cold gas reservoirs at other halo masses. Galaxies residing in lower mass haloes are dominated by their cold gas content, but have very low molecular fractions. As a result a relatively small amount of gas is available for the formation of stars. This suggests an interesting physical scenario, in which these galaxies are efficient at cooling gas onto their disc, but physics internal to the galaxies prevents them from forming molecules. That is, low densities, stellar winds and supernova feedback seem to be efficient at disrupting $H_2$ formation, and are not (nor do they need to be) efficient at suppressing cooling for HI even at $z = 0$.

We have shown that galaxies residing in haloes larger than $10^{12}\,{\rm M}_\odot$ cannot build up gas reservoirs much larger than a few times $10^{10}\,{\rm M}_\odot$. We also see this in the time evolution of the gas content in galaxies (Figure 16). This is supported by the decline in cold gas fractions as a function of halo mass seen at all redshifts. Interestingly, the cold gas molecular fraction is roughly constant for haloes with masses larger than $10^{12}\,{\rm M}_\odot$ as is the star formation efficiency of the galaxies. This constancy in $H_2$ fraction is supported by the drop in cold gas fraction and $\frac{\rm M_{H2}}{\rm M_\star}$ for galaxies with masses $M_\star > 10^{10}\,{\rm M}_\odot$. This upper limit in cold gas molecular fraction provides an explanation for the plateau in SFE for galaxies with stellar masses $M_\star > 10^{10}\,{\rm M}_\odot$.

Haloes of masses $\sim 10^{12}\,{\rm M}_\odot$ have stored approximately 20–30 per cent of their baryons in stars and cold gas in the central galaxy. Haloes with lower and higher masses are less efficient in bringing the baryons down to their central galaxy. This supports the findings that star-forming and passive galaxies have significant ionized gas reservoirs in their haloes (Tumlinson et al. 2011; Bordoloi et al. 2014; Werk et al. 2014). The masses of these cold gas reservoirs are comparable for star-forming and passive galaxies (Thom et al. 2012). All of these results tie in with a picture in which heating processes (such as supernovae feedback, active galactic nuclei feedback, and shock heating) prevent the build-up of large amounts of cold gas onto the galaxies. Especially once a host halo reaches a mass of $\sim 10^{12}\,{\rm M}_\odot$ the number of baryons not stored in the central galaxy grows rapidly (Figure 16). However, once cooled onto a galaxy the local gas conditions determine the efficiency of the cold gas to become molecular and form stars.

We note that our present conclusions are based on our assumptions that $H_2$ traces SF and that the partitioning of cold gas in H I and $H_2$ only depends on the pressure acting on the gas. Processes such as ram-pressure stripping and the destruction of molecules by AGN feedback also affect the gaseous and molecular content of galaxies. Furthermore, dust grains and metals play an important role as the catalysts and coolants for $H_2$ formation. This is especially important in low-density and low-metallicity environments (Krumholz & Dekel 2012; Popping, Somerville & Trager 2014) and would further suppress the formation of molecules in the lowest mass haloes.

### 4.5 Excess of galaxies with low H I masses

Our model correctly reproduces the H I and $H_2$ content of local galaxies and the observed $H_2$ mass function. We obtain good agreement with the observed H I mass function for H I-rich galaxies ($M_{\rm HI} > 10^{9.0}\,{\rm M}_\odot$), but overpredict the number of galaxies with lower H I masses. The galaxies responsible for this excess have low stellar masses ($M_\star < 10^{8.5}\,{\rm M}_\odot$). To first order the steep slope at the low-mass end of the H I mass function is a result of the steep slope in the predicted stellar mass function (Behroozi, Wechsler & Conroy 2013b), corresponding with an upturn in the observed stellar mass function below $10^{8.5}{\rm M}_\odot$ (Baldry, Glazebrook & Driver 2008). The exact shape of the stellar mass function in this regime is quite uncertain due to incompleteness of low-surface-brightness galaxies (Baldry et al. 2012).

Nevertheless, it is highly uncertain whether the poor number statistics of low-surface-brightness galaxies can fully account for the severe mismatch between the observed and inferred H I mass function. For galaxies with low stellar masses the observed ratio between the H I and stellar mass of galaxies has a steep faint-end slope (McGaugh 2012; Zhang et al. 2012). The stellar mass function has a negative slope with stellar mass in the same mass regime (Baldry, Glazebrook & Driver 2008; Baldry et al. 2012). It is then hard to reconcile that the observed H I mass function is relatively flat at H I masses of $10^{8-9}\,{\rm M}_\odot$ (Zwaan et al. 2005; Martin et al. 2010). We can only explain for this if the H I-to-stellar mass ratio for galaxies with low stellar masses is not as well behaved as suggested by current surveys and we are missing a significant population of H I poor galaxies at low stellar masses (for example dwarf spheroidal galaxies). Given the steep slope we find in the $H_2$ mass function at $M_\star < 10^8\,{\rm M}_\odot$ it is not unlikely that these H I poor galaxies are also diluted from $H_2$.

We note that our assumption for exponential discs may not be appropriate for galaxies with H I masses smaller than $10^9\,{\rm M}_\odot$. Kelvin et al. (2014) showed that below stellar masses of $10^9\,{\rm M}_\odot$ the stellar mass function is mostly made up by irregular galaxies. The different distribution of gas in these galaxies compared to our assumption of exponential discs can have a significant effect on the inferred H I masses. Furthermore, the stellar and gas sizes of these low mass galaxies are observationally not well constrained. A better understanding of the mass and distribution of H I for a large sample of galaxies with low stellar masses can improve the situation and resolve the discrepancy between the observed and inferred H I mass function at $z = 0$.

## 5 SUMMARY & CONCLUSIONS

In this paper we have presented a new semi-empirical approach to infer the H I and $H_2$ content of galaxies as a function of redshift and host halo mass. All data results in this paper are available for download online.[3] We summarize our main results below:

- There is weak evolution in the H I content and H I mass function of galaxies at redshifts $z < 1.5$ (less than half a dex in H I mass), whereas the $H_2$ content and mass function evolve strongly in this redshift range (more than an order of magnitude in $H_2$ mass at $z < 1.5$). This behavior originates in a self-regulated equilibrium in the H I mass of galaxies controlled by the amount of cold gas available and its partitioning into an atomic and molecular part.
- The cold gas fraction of galaxies decreases as a function of stellar mass and time. The relative $H_2$ content of galaxies decreases with stellar mass and redshift as well, but more rapidly (from 0.75 to almost zero at stellar masses of $10^{10}\,{\rm M}_\odot$).
- Massive galaxies consume and/or expel their cold gas content earlier than less massive galaxies. Galaxies with a stellar mass of $10^{11}\,{\rm M}_\odot$ are dominated by their stellar content at $z = 3$, whereas galaxies with a stellar mass of $10^9\,{\rm M}_\odot$ still have a gas fraction of 50% at $z = 0$. We find a rapid decrease in cold gas fractions at $z < 1.5$. This supports a picture in which the accretion of new cold material onto galaxies slows down at these redshifts, possibly due to shock heating or heating from active galactic nuclei feedback of the sparse infalling gas.
- The SFR-to-gas mass ratio, i.e. the star formation efficiency, decreases by more than an order of magnitude from $z = 3$ to $z = 0$. This is driven by the declining trend of molecular fractions with time, allowing relatively less gas to form stars.
- We confirm that when adopting a $H_2$-based star-formation relation one can fuel the peak in cosmic SFR at $z \sim 2$ and simultaneously reproduce the weak evolution in $\Omega_{\rm HI}$ during the same epoch.
- Galaxies residing in haloes of mass $\sim 10^{12}\,{\rm M}_\odot$ are most efficient in attaining cold gas *and* forming molecules. The combination of these two effects explains for the high star-formation efficiencies of galaxies in haloes in the same mass range. In haloes of mass $\sim 10^{12}\,{\rm M}_\odot$, roughly 30 percent of the baryons is locked up in cold gas and stars within the central galaxy at $z = 3$ . This number decreases to roughly 17 percent for galaxies residing in haloes with the same mass at $z = 0$. Galaxies in lower-mass haloes have significant cold gas reservoirs, but only a minor fraction of their gas is molecular. Heating processes prevent the buildup of large gas reservoirs in galaxies residing in more massive haloes.

These results serve as predictions for future surveys of the atomic and molecular content of galaxies. We look forward to observations from new and upcoming radio and sub-mm facilities such as ALMA, SKA and its pathfinders MeerKat and ASKAP that will confront our results. The inferred gas masses presented do not depend on unknown recipes for feedback and heating processes, but on galaxy properties that by construction are representative of real galaxies. We anticipate that semi-empirical efforts such as presented here have the potential to break degeneracies between different physical recipes, allowing for a better understanding of the fueling and stellar-buildup of galaxies.

## ACKNOWLEDGMENTS

We thank the anonymous referee for constructive comments. We thank Romeel Davé, Thijs van der Hulst, Andrey Kravtsov, Houjun Mo, Rachel Somerville, Marco Spaans,

[3] `http://www.eso.org/~gpopping/Gergo_Poppings_Homepage/Data.html`

Scott Trager, Arjen van der Wel, and Cathy White for stimulating discussions and comments, and Amber Bauermeister, Matthew Bothwell, Claudia Lagos, Danail Obreschkow, and Fabian Walter for providing data. GP acknowledges NOVA (Nederlandse Onderzoekschool voor Astronomie) for funding. PB was supported by a Giacconi Fellowship through the Space Telescope Science Institute, which is operated by the Association of Universities for Research in Astronomy, Incorporated, under NASA contract NAS5-26555. We also thank galaxies for being awesome.

**References**

Baldry I. K. et al., 2012, MNRAS, 421, 621
Baldry I. K., Glazebrook K., Driver S. P., 2008, MNRAS, 388, 945
Bauermeister A. et al., 2013, ApJ, 768, 132
Bauermeister A., Blitz L., Ma C.-P., 2010, ApJ, 717, 323
Behroozi P. S., Conroy C., Wechsler R. H., 2010, ApJ, 717, 379
Behroozi P. S., Wechsler R. H., Conroy C., 2013a, ApJ, 762, L31
—, 2013b, ApJ, 770, 57
Berry M., Somerville R. S., Haas M. R., Gawiser E., Maller A., Popping G., Trager S. C., 2014, MNRAS, 441, 939
Bigiel F., Blitz L., 2012, ApJ, 756, 183
Bigiel F., Leroy A., Walter F., Brinks E., de Blok W. J. G., Madore B., Thornley M. D., 2008, AJ, 136, 2846
Birnboim Y., Dekel A., 2003, MNRAS, 345, 349
Blitz L., Rosolowsky E., 2006, ApJ, 650, 933
Bordoloi R. et al., 2014, ApJ, 796, 136
Boselli A., Cortese L., Boquien M., Boissier S., Catinella B., Lagos C., Saintonge A., 2014, A&A, 564, A66
Bothwell M. S., Kennicutt R. C., Lee J. C., 2009, MNRAS, 400, 154
Bothwell M. S. et al., 2014, MNRAS, 445, 2599
Brammer G. B. et al., 2011, ApJ, 739, 24
Braun R., 2012, ApJ, 749, 87
Bryan G. L., Norman M. L., 1998, ApJ, 495, 80
Catinella B., Cortese L., 2015, MNRAS, 446, 3526
Catinella B., Haynes M. P., Giovanelli R., Gardner J. P., Connolly A. J., 2008, ApJ, 685, L13
Catinella B. et al., 2013, MNRAS, 436, 34
—, 2012, A&A, 544, A65
—, 2010, MNRAS, 403, 683
Chabrier G., 2003, PASP, 115, 763
Christensen C., Quinn T., Governato F., Stilp A., Shen S., Wadsley J., 2012, MNRAS, 425, 3058
Conroy C., Wechsler R. H., 2009, ApJ, 696, 620
Daddi E. et al., 2010, ApJ, 713, 686
Davé R., Finlator K., Oppenheimer B. D., 2011, MNRAS, 416, 1354
Davé R., Katz N., Oppenheimer B. D., Kollmeier J. A., Weinberg D. H., 2013, MNRAS, 434, 2645
Dekel A., Birnboim Y., 2006, MNRAS, 368, 2
Dekel A. et al., 2009, Nature, 457, 451
Delhaize J., Meyer M. J., Staveley-Smith L., Boyle B. J., 2013, MNRAS, 433, 1398
Dutton A. A., van den Bosch F. C., Dekel A., 2010, MNRAS, 405, 1690
Erb D. K., Steidel C. C., Shapley A. E., Pettini M., Reddy N. A., Adelberger K. L., 2006, ApJ, 646, 107
Fernández X. et al., 2013, ApJ, 770, L29
Fontanot F., De Lucia G., Monaco P., Somerville R. S., Santini P., 2009, MNRAS, 397, 1776
Fu J., Guo Q., Kauffmann G., Krumholz M. R., 2010, MNRAS, 409, 515
Fu J., Kauffmann G., Li C., Guo Q., 2012, MNRAS, 424, 2701
Geach J. E., Smail I., Moran S. M., MacArthur L. A., Lagos C. d. P., Edge A. C., 2011, ApJ, 730, L19
Genzel R. et al., 2010, MNRAS, 407, 2091
Giovanelli R. et al., 2005, AJ, 130, 2598
Grogin N. A. et al., 2011, ApJS, 197, 35
Guimarães R., Petitjean P., de Carvalho R. R., Djorgovski S. G., Noterdaeme P., Castro S., Poppe P. C. D. R., Aghaee A., 2009, A&A, 508, 133
Guo Q., White S., Li C., Boylan-Kolchin M., 2010, MNRAS, 404, 1111
Helfer T. T., Thornley M. D., Regan M. W., Wong T., Sheth K., Vogel S. N., Blitz L., Bock D., 2003, ApJS, 145, 259
Hopkins A. M., Beacom J. F., 2006, ApJ, 651, 142
Hunter D. A. et al., 2012, AJ, 144, 134
Kelvin L. S. et al., 2014, MNRAS, 444, 1647
Kennicutt, Jr. R. C., 1998, ApJ, 498, 541
Kereš D., Katz N., Fardal M., Davé R., Weinberg D. H., 2009, MNRAS, 395, 160
Kereš D., Katz N., Weinberg D. H., Davé R., 2005, MNRAS, 363, 2
Kereš D., Yun M. S., Young J. S., 2003, ApJ, 582, 659
Koekemoer A. M. et al., 2011, ApJS, 197, 36
Kravtsov A. V., 2013, ApJ, 764, L31
Krumholz M. R., Dekel A., 2012, ApJ, 753, 16
Kuhlen M., Krumholz M. R., Madau P., Smith B. D., Wise J., 2012, ApJ, 749, 36
Lagos C. D. P., Baugh C. M., Lacey C. G., Benson A. J., Kim H.-S., Power C., 2011, MNRAS, 1776
Leroy A. K. et al., 2009, AJ, 137, 4670
Leroy A. K., Walter F., Brinks E., Bigiel F., de Blok W. J. G., Madore B., Thornley M. D., 2008, AJ, 136, 2782
Lu Y. et al., 2014a, ApJ, 795, 123
Lu Z., Mo H. J., Lu Y., 2014, ArXiv e-prints 1408.2640
Lu Z., Mo H. J., Lu Y., Katz N., Weinberg M. D., van den Bosch F. C., Yang X., 2014b, MNRAS, 439, 1294
—, 2014c, ArXiv e-prints 1406.5068
Madau P., Dickinson M., 2014, ARA&A, 52, 415
Mannucci F. et al., 2009, MNRAS, 398, 1915
Martin A. M., Papastergis E., Giovanelli R., Haynes M. P., Springob C. M., Stierwalt S., 2010, ApJ, 723, 1359
McGaugh S. S., 2012, AJ, 143, 40
Moster B. P., Naab T., White S. D. M., 2013, MNRAS, 428, 3121
Moster B. P., Somerville R. S., Maulbetsch C., van den Bosch F. C., Macciò A. V., Naab T., Oser L., 2010, ApJ, 710, 903
Muñoz J. A., Peeples M. S., 2014, ArXiv e-prints 1404.1915
Noeske K. G. et al., 2007, ApJ, 660, L43
Noterdaeme P. et al., 2012, A&A, 547, L1
Obreschkow D., Croton D., De Lucia G., Khochfar S., Rawlings S., 2009, ApJ, 698, 1467

Obreschkow D., Rawlings S., 2009, MNRAS, 394, 1857
Oppenheimer B. D., Davé R., Kereš D., Fardal M., Katz N., Kollmeier J. A., Weinberg D. H., 2010, MNRAS, 406, 2325
Peeples M. S., Somerville R. S., 2013, MNRAS, 428, 1766
Péroux C., Dessauges-Zavadsky M., D'Odorico S., Sun Kim T., McMahon R. G., 2005, MNRAS, 363, 479
Popping G., Caputi K. I., Somerville R. S., Trager S. C., 2012, MNRAS, 425, 2386
Popping G., Pérez-Beaupuits J. P., Spaans M., Trager S. C., Somerville R. S., 2014, MNRAS, 444, 1301
Popping G., Somerville R. S., Trager S. C., 2014, MNRAS, 442, 2398
Prochaska J. X., Wolfe A. M., 2009, ApJ, 696, 1543
Rafieferantsoa M., Davé R., Anglés-Alcazar D., Katz N., Kollmeier J. A., Oppenheimer B. D., 2014, ArXiv 1408.2531
Rao S. M., Turnshek D. A., Nestor D. B., 2006, ApJ, 636, 610
Reddick R. M., Wechsler R. H., Tinker J. L., Behroozi P. S., 2013, ApJ, 771, 30
Riechers D. A., Hodge J., Walter F., Carilli C. L., Bertoldi F., 2011, ApJ, 739, L31
Saintonge A. et al., 2011, MNRAS, 415, 32
Schruba A. et al., 2011, AJ, 142, 37
Scoville N. et al., 2007, ApJS, 172, 1
Somerville R. S., Davé R., 2014, ArXiv 1412.2712
Tacconi L. J. et al., 2010, Nature, 463, 781
—, 2013, ApJ, 768, 74
Thom C. et al., 2012, ApJ, 758, L41
Thompson R., Nagamine K., Jaacks J., Choi J.-H., 2014, ApJ, 780, 145
Tinker J., Kravtsov A. V., Klypin A., Abazajian K., Warren M., Yepes G., Gottlöber S., Holz D. E., 2008, ApJ, 688, 709
Tinsley B. M., 1980, Fund. Cosmic Phys., 5, 287
Tumlinson J. et al., 2011, Science, 334, 948
van der Wel A. et al., 2014, ApJ, 788, 28
Verheijen M., van Gorkom J. H., Szomoru A., Dwarakanath K. S., Poggianti B. M., Schiminovich D., 2007, ApJ, 668, L9
Walter F., Brinks E., de Blok W. J. G., Bigiel F., Kennicutt R. C., Thornley M. D., Leroy A., 2008, AJ, 136, 2563
Walter F. et al., 2014, ApJ, 782, 79
Wang L., Jing Y. P., 2010, MNRAS, 402, 1796
Weinmann S. M., Pasquali A., Oppenheimer B. D., Finlator K., Mendel J. T., Crain R. A., Macciò A. V., 2012, MNRAS, 426, 2797
Werk J. K. et al., 2014, ApJ, 792, 8
White C. E., Somerville R. S., Ferguson H. C., 2014, ArXiv e-prints 1407.1850
Wong T., Blitz L., 2002, ApJ, 569, 157
Yang X., Mo H. J., van den Bosch F. C., 2003, MNRAS, 339, 1057
Yang X., Mo H. J., van den Bosch F. C., Zhang Y., Han J., 2012, ApJ, 752, 41
Zafar T., Péroux C., Popping A., Milliard B., Deharveng J.-M., Frank S., 2013, A&A, 556, A141
Zhang H.-X., Hunter D. A., Elmegreen B. G., Gao Y., Schruba A., 2012, AJ, 143, 47
Zwaan M. A., Meyer M. J., Staveley-Smith L., Webster R. L., 2005, MNRAS, 359, L30

## APPENDIX A: GAS EVOLUTION FOR INDIVIDUAL GALAXIES

We presented the evolution of the cold gas content of galaxies as a function of their $z = 0$ host halo mass in Figure 16. The presented results are based on median accretion histories, smoothing over the accretion and star formation histories of individual galaxies. We present the evolution of cold gas content for individual mass accretion histories in Figure A1. The trends of cold gas, H I, and $H_2$ with time are similar to the trends showed in Figure 16 but with a wider spread.

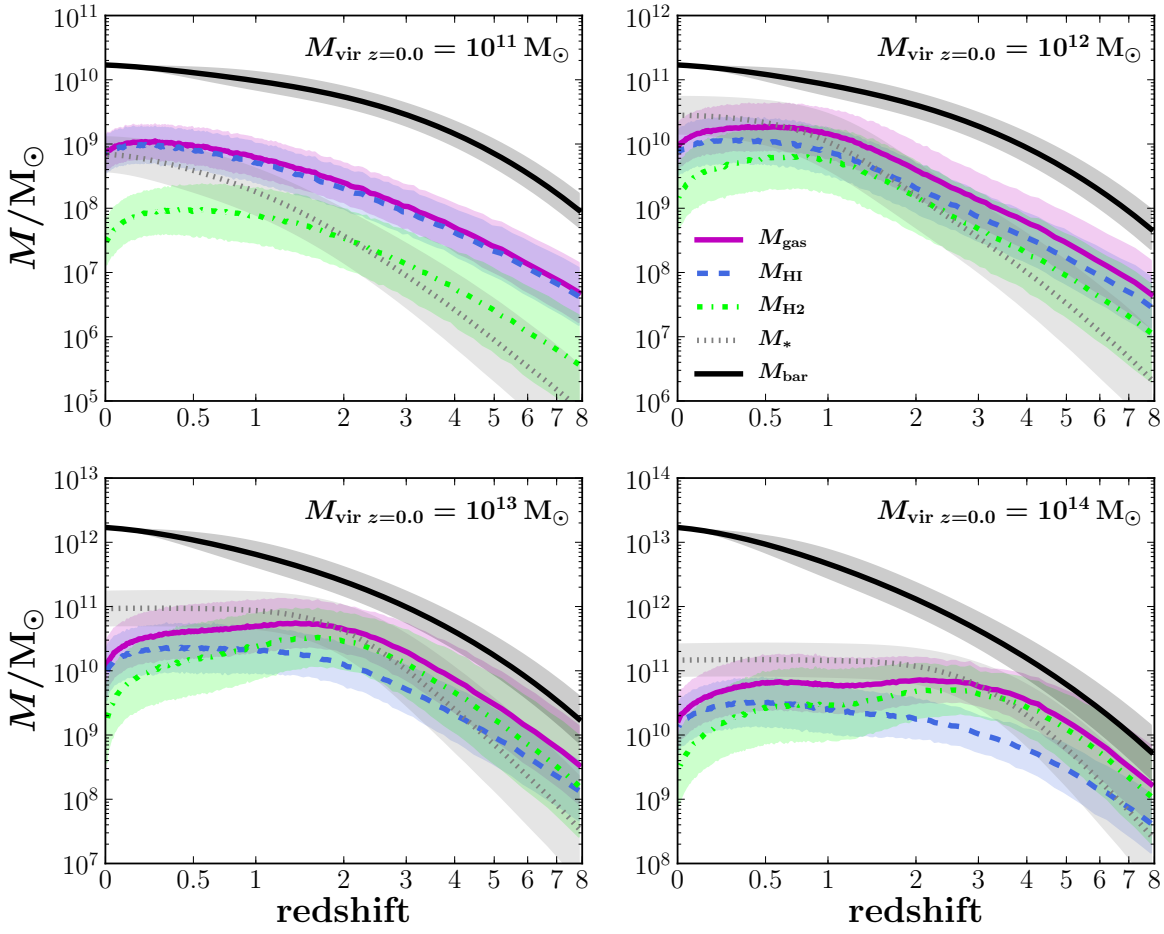


**Figure A1.** Time evolution of the total cold gas (solid purple), H I (dashed blue), $H_2$ (dashed dotted green), stellar (dashed grey) and baryonic mass of the halo (solid black) for haloes as a function of their $z = 0$ halo mass for individual mass accretion histories (rather than the median). The shaded regions show the one-sigma posterior distributions.